

# CHALMERS



## Design and Evaluation of an Active Rectifier for a 4.1 MW Off-Shore Wind Turbine

Subtitle

*Master of Science Thesis*

**SHAMIM KESHAVARZ**

Department of Energy and Environment  
*Division of Electric Power Engineering*  
CHALMERS UNIVERSITY OF TECHNOLOGY  
Göteborg, Sweden, 2011



# Design and Evaluation of an Active Rectifier for a 4.1 MW Off-Shore Wind Turbine

Master of Science Thesis

SHAMIM KESHAVARZ

Department of Energy and Environment  
*Division of Electric Power Engineering*  
CHALMERS UNIVERSITY OF TECHNOLOGY

Göteborg, Sweden 2011

Design and Evaluation of an Active Rectifier for a 4.1 MW Off-Shore Wind Turbine

Master of Science Thesis  
SHAMIM KESHAVARZ

© SHAMIM KESHAVARZ, 2011

Department of Energy and Environment  
Division of Electric Power Engineering  
Chalmers University of Technology  
SE-412 96 Göteborg  
Sweden  
Telephone: + 46 (0)31-772 1000

## **Abstract**

In this master thesis, the design of an AC-DC converter for an off-shore wind turbine is evaluated from a loss point of view. For this project, a 4.1 MW Permanent Magnet Synchronous machine will be used as a generator of the wind turbine.

For the active AC-DC conversion, active semiconductors can be used (MOSFET or IGBT). Since we are dealing with high voltage, IGBTs will be implemented based on their performance and advantages over other semiconductors.

Afterwards, the efficiency, and power factor of the converter will be evaluated, as well as the calculation of the switching losses of the IGBTs as a function of the switching frequency. For the latter, different switching frequencies will be tested in order to evaluate the performance of the converter.

Selection of the IGBT is another important part of the project which will be done in accordance to the voltage level, current consumption and losses.

MATLAB 7.0 is the software that will be used for this project.

This master thesis is primarily thought for an HVDC application, and here the scope is to rectify the current of the output of a permanent magnet synchronous generator used as a wind turbine generator.

**Keywords:** Active Rectifier, IGBT, Permanent Magnet Synchronous Generator.

## **Acknowledgments**

I would like to give special thanks to my supervisor Torbjörn Thiringer for his great support and constant guidance during this master thesis.

I want to thank also Poopak Roshanfekr for her collaboration in this project, and to all the friends and people that in one way or another gave their time with ideas and tips for the development of this thesis.

I want to appreciate the encouragement and endless love that my parents (Bijan and Bahiyeh) always gave to me and for their constant advice in all affairs of my life.

# Contents

<b>List of Symbols, Subscripts and Abbreviations .....</b>	<b>V</b>
<b>1 Introduction .....</b>	<b>1</b>
1.1 Problem Overview .....	1
1.2 Overview of Previous Work.....	1
1.3 Purpose of this Report.....	2
1.4 Layout of this Report .....	2
<b>2 Theory.....</b>	<b>3</b>
2.1 Active Rectifier .....	3
2.1.1 Definition .....	3
2.1.2 IGBT fundamentals.....	8
2.2 Modeling of Permanent Magnet Synchronous Machine (PMSG).....	11
2.2.1 Introduction and Definition.....	11
2.2.2 Mathematical Model .....	12
2.2.3 Machine Design Model.....	14
<b>3 Case Set-Up.....</b>	<b>17</b>
3.1 Case Specification for Permanent Magnet Synchronous Generator .....	17
3.2 Active Rectifier Circuit Diagram for PMSG .....	17
3.3 Specification of the Power Electronic System (IGBT's Specification).....	18
<b>4 Analysis (Results and Discussions) .....</b>	<b>23</b>
4.1 Verification of main operation with MATLAB.....	23
4.2 Calculation of Losses as function of Switching Frequency.....	26
<b>5 Conclusions .....</b>	<b>37</b>
<b>6 Future Work .....</b>	<b>39</b>
<b>7 Bibliography.....</b>	<b>41</b>



## List of Symbols, Subscripts and Abbreviations

### Abbreviations

PMSG	Permanent Magnet Synchronous Generator
PMSM	Permanent Magnet Synchronous Machine
EMSM	Electrically Magnetized Synchronous Machine
IGBT	Insulated Gate Bipolar Transistor
MOSFET	Metal Oxide Semiconductor Field-Effect Transistor
PWM	Pulse Width Modulation
BJT	Bipolar Junction Transistor
SOA	Safe Operating Area
NPT	Non-Punch Through
PT	Punched Through

### Symbols

$u_a$	Line Voltage
$E_m$	Amplitude of line-to-neutral voltage
$i_a$	Line current
$I_m$	Amplitude of line-to-neutral current
$v^s$	Voltage space vector
$i^s$	Current space vector
$v_\alpha$	Voltage space vector alpha component
$v_\beta$	Voltage space vector beta component
$v_a$	Voltage space vector line component
$K$	Scaling factor
$S_a$	Switching state of converter (for phase a)
$R$	Resistance
$L$	Inductance
$C$	Capacitance
$i_{load}$	Load current
$u_\alpha$	Voltage alpha component
$u_\beta$	Voltage beta component
$i_\alpha$	Current alpha component
$i_\beta$	Current beta component
$v_{dq}$	Voltage expressed in dq coordinates
$i_d$	Current d-component
$i_q$	Current q-component
$u_d$	Voltage d-component
$u_q$	Voltage q-component
$U_{sdq}$	Converter voltage in dq-coordinates system
$\theta$	Transformer angle
$\varphi$	Phase angle
$P$	Active Power
$Q$	Reactive Power
$v^{dq}$	Voltage space vector in dq coordinates
$i^{dq}$	Current space vector in dq coordinates
$V_{LL(RMS)}$	Line-to-line RMS voltage
$V_{LN(peak)}$	Line-to-neutral peak voltage
$V_{LN(RMS)}$	Line-to-neutral RMS voltage
$V_{DC}$	DC-link voltage
$V_{DCmin}$	Minimum DC-link voltage

$\underline{u}_s^s$	Stator voltage vector in stationary coordinates
$R_s$	Stator resistance
$\underline{i}_s^s$	Stator current vector in stationary coordinates
$\underline{\psi}_s^s$	Stator flux in stationary coordinates
$L_{s\lambda}$	Leakage inductance
$L_m$	Mutual inductance
$\psi_m$	Mutual flux linkage
$\omega_r$	Electrical rotor speed
$L_s$	Stator inductance
$T_e$	Electrical Torque
$n_p$	Number of pole pairs
$u_{s\alpha}$	Converter voltage vector alpha component
$u_{s\beta}$	Converter voltage vector beta component
$i_{s\alpha}$	Converter current vector alpha component
$i_{s\beta}$	Conveter current vector beta component
$J$	Total inertia of machine
$T_l$	Load torque
$\underline{u}_s$	Stator voltage vector
$\underline{i}_s$	Stator current vector
$u_{sd}$	Converter voltage vector d component
$u_{sq}$	Converter voltage vector q component
$i_{sd}$	Converter current vector d component
$i_{sq}$	Converter current vector q component
$L_{sd}$	Stator inductance in d direction
$L_{sq}$	Stator inductance in q direction
$\theta_r$	Rotor position
$\phi_r$	Angle of the flux linkage vector originated from magnet in the rotor
$\theta_s$	Stator flux linkage angle
$e$	Back-emf of machine
$f$	Frequency
$f_{sw}$	Switching frequency
$V_{GE}$	Gate-emitter voltage
$V_{GE(th)}$	Gate-emitter threshold voltage
$V_{CE(ON)}$	On-state collector-emitter voltage drop
$R_{CE(ON)}$	On-state resistance of IGBT
$E_{rec}$	Reverse recover energy of freewheeling diode
$R_F$	Forward resistance of freewheeling diode
$V_F$	Forward voltage of freewheeling diode
$E_{sw\_IGBT(ON)}$	Switching energy of IGBT during turn-on
$E_{sw\_IGBT(OFF)}$	Switching energy of IGBT during turn-off
$OV$	Overvoltage Factor
$V_{cc}$	Voltage taken by each IGBT
$M$	Amplitude modulation

# 1 Introduction

## 1.1 Problem Overview

Over the past few years, wind energy has become one of the fastest growing sources of electricity and one of the fastest growing markets in the world today. The re-emergence of the wind as a significant source of the world's energy must be ranked as one of the significant developments of the late 20th century. These growth trends can be linked to the multi-dimensional benefits associated with wind energy such as:

- The electricity produced from wind power is said to be “clean energy” because of its lack of greenhouse gas during operation.
- Wind power is a cost-competitive source of electricity, largely due to technological advancements, as well as economies of a large scale, as more of these machines are manufactured and put online around the world.
- Maintenance-low operation: Wind turbines only require a semi-annual based maintenance or employment of operations personnel; compared to steam and gas turbine-based alternator systems, lower maintenance or operational costs are incurred.

Numerous wind farm projects are being constructed around the globe with both offshore and onshore developments in Europe and primarily large onshore developments in North America.

Onshore wind turbines are frequently installed in upland terrain to seize higher wind speeds. However, wind farms permitting and siting onshore can be difficult as high wind-speed sites often have a high visual amenity value, noise and affect the environment.

Offshore wind turbines, particularly larger wind farms, should generally take place more than 5 km from land to reduce environmental impact. The advantages of offshore wind farms include reduced visual intrusion and acoustic noise impact and also lower wind turbulence with higher average wind speeds. The obvious disadvantages are the higher costs of constructing and operating wind turbines offshore, and the longer power cables that must be used to connect the wind farm to the terrestrial power grid. More information about overview and generalities of wind energy can be found in [1-4].

This project is focused on remote offshore application, where a DC transmission must be used. There is a need to rectify the current coming from the generator using semiconductors (in our case IGBTs). Afterwards, the DC voltage will be boosted to reach the HVDC level in order to transmit power in a more efficient and economical way.

Several studies of HVDC transmission have been made that show that with this technology, the costs and losses can be lowered compared to classical set-ups and that the controllability and efficiency increase. For more information refer to [5-7].

## 1.2 Overview of Previous Work

There have been several configurations of wind parks that have been implemented in wind power, which can be seen in more detail in [8-10] and also some specific work related to AC-DC conversion, [11] which is related to this master thesis. Also, [12] and [13] show different DC High Voltage connections for wind farms and the most recent previous works related to this master thesis.

So, this work will show an implementation of a configuration of a wind park with a permanent magnet synchronous machine as the generator of the wind turbine and an active rectifier, which is an AC-DC converter with IGBTs as the switches of the converter.

### **1.3 Purpose of this Report**

The purpose of this work is to design an active rectifier for a 4.1 MW off-shore wind turbine that will be used for HVDC application. In more precise words, the design of a converter using active power semiconductors (IGBTs) for wind power application is fulfilled. The efficiency, power factor performance, selection of IGBT as well as calculation of losses in the power semiconductors of the converter are targets of the investigations.

### **1.4 Layout of this Report**

In Chapter 2, some theory background of the features, characteristics, classifications, advantages and disadvantages of active rectifiers and IGBTs is shown. For the permanent magnet synchronous generator an introduction, classification, mathematical model, machine design model and control system that it will be implemented for the switches of the converter will be presented.

In Chapter 3, the case set-up is shown. The general data of the generator that will be implemented is presented, as well as the circuit diagram of the active rectifier and the specification for the selected IGBT that will be used for the converter. All calculations are presented here.

In Chapter 4, the results are shown. Here, the efficiency, power factor and loss calculation as function of the switching frequency of the active rectifier are presented. Also some analysis regarding the performance of the converter is discussed.

In Chapter 5 and 6, the conclusions and future work are presented.

And finally, Chapter 7 shows the bibliography.

## 2 Theory

### 2.1 Active Rectifier

#### 2.1.1 Definition

Three-Phase controlled rectifiers can be classified from the point of view of the commutation process as Line Commutated Controlled Rectifiers (Thyristor Rectifiers) and Force Commutated PWM Rectifiers [14]. A more detailed classification of three-phase rectifier systems can be found in [15].

Force commutated rectifiers are built with semiconductors with gate-turn-off capability. This allows full control of the converter, because valves can be switched ON and OFF whenever it is required. Active rectifiers are located in this last category. This allows the commutation of the valves hundreds of times in one fundamental period, which is not possible with line commutated rectifiers, where thyristors are switched ON once a cycle.

The advantages using this feature are: a) the current or voltage can be modulated (Pulse Width Modulation or PWM), generating less harmonic contamination; b) power factor can be controlled.

There are two types of force-commutated three-phase rectifiers: a) current source rectifier, where power reversal is by dc voltage reversal; and b) as a voltage source rectifier where power reversal is by current reversal at the dc link.

So, we can define the *Active Rectifier* as “A non-isolated AC-DC converter that uses actively controlled switches such as MOSFETs or IGBTs instead of diodes or thyristors in order to rectify the voltage/current with two key benefits: output voltage (DC-link) regulation and AC input harmonic reduction. The converter is inherently bi-directional, and thus the DC side can be output or input.”

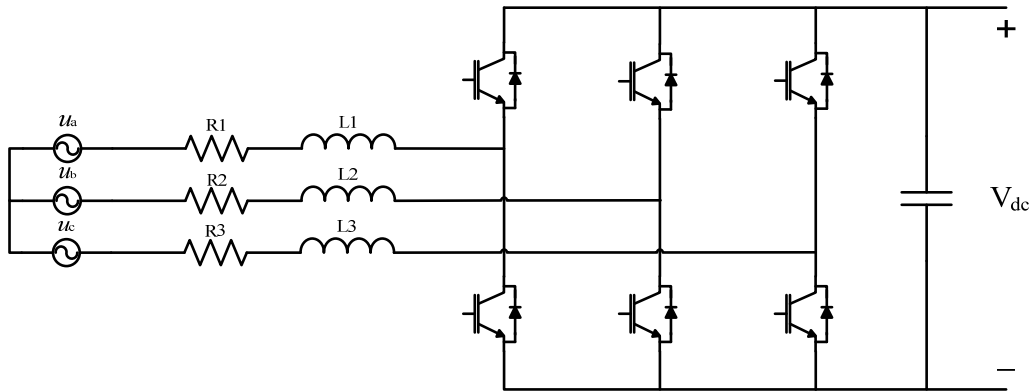


**Figure 2.1:** Three-Phase Active Rectifier topology: Voltage Source Rectifier.

The topology shown in figure 2.1 is able to perform regulation of DC output voltage, low harmonic distortion of line current, power factor correction and bidirectional power flow.

The main philosophy of the DC-systems is that all wind turbines shall have a fix output voltage regardless of the wind speed in steady-state to simplify the DC-grid connection. One of the benefits of this topology (see figure 2.1) is that for example if a DC-DC converter is installed after the dc-link, the active rectifier keeps the input voltage to the DC-DC converter constant.

The mathematical model of the three-phase line voltages and currents are [16],

$$u_a = E_m \cos(\omega t) \quad (2.1)$$

$$u_b = E_m \cos\left(\omega t - \frac{2\pi}{3}\right) \quad (2.2)$$

$$u_c = E_m \cos\left(\omega t - \frac{4\pi}{3}\right) \quad (2.3)$$

$$i_a = I_m \cos(\omega t + \varphi) \quad (2.4)$$

$$i_b = I_m \cos\left(\omega t + \varphi - \frac{2\pi}{3}\right) \quad (2.5)$$

$$i_c = I_m \cos\left(\omega t + \varphi - \frac{4\pi}{3}\right) \quad (2.6)$$

Since there is no neutral connection,

$$i_a + i_b + i_c = 0 \quad (2.7)$$

The three-phase system can be described using the  $\alpha\beta$  model. Therefore, we define a space vector as:

$$v^s(t) = v_\alpha(t) + jv_\beta(t) \quad (2.8)$$

$$v^s(t) = \frac{2}{3}K \left( v_a(t) + v_b(t)e^{j\frac{2\pi}{3}} + v_c(t)e^{j\frac{4\pi}{3}} \right) \quad (2.9)$$

Where K is a scaling constant (If amplitude invariant transformation is used,  $K=1$ , RMS-invariant  $K=1/\sqrt{2}$  or power invariant  $K=\sqrt{3/2}$ ).

Rectifier ABC-Model:

$$u_{Sab} = (S_a - S_b)u_{dc} \quad (2.10)$$

$$u_{Sbc} = (S_b - S_c)u_{dc} \quad (2.11)$$

$$u_{Sca} = (S_c - S_a)u_{dc} \quad (2.12)$$

With  $S_i$  being the switching function defined by 1 if the upper switch is ON and 0 if the bottom switch is ON with phase  $i = a, b, c$ , the following voltages are found:

$$u_{Sa} = f_a u_{dc} \quad (2.13)$$

$$u_{Sb} = f_b u_{dc} \quad (2.14)$$

$$u_{Sc} = f_c u_{dc} \quad (2.15)$$

$$f_a = S_a - S^* \quad (2.16)$$

$$f_a = S_a - \frac{1}{3}(S_a + S_b + S_c) \quad (2.17)$$

$$f_a = \frac{2S_a - (S_b + S_c)}{3} \quad (2.18)$$

$$f_b = \frac{2S_b - (S_a + S_c)}{3} \quad (2.19)$$

$$f_c = \frac{2S_c - (S_a + S_b)}{3} \quad (2.20)$$

Now we define the active rectifier by four equations, one for each phase (voltage) and one for the current (dc-link)

$$\begin{bmatrix} u_a \\ u_b \\ u_c \end{bmatrix} = R \begin{bmatrix} i_a \\ i_b \\ i_c \end{bmatrix} + L \frac{d}{dt} \begin{bmatrix} i_a \\ i_b \\ i_c \end{bmatrix} + \begin{bmatrix} u_{Sa} \\ u_{Sb} \\ u_{Sc} \end{bmatrix} \quad (2.21 - 2.23)$$

as well as,

$$C \frac{du_{dc}}{dt} = S_a i_a + S_b i_b + S_c i_c - i_{load} \quad (2.24)$$

The transformation from three-phase to  $\alpha\beta$  and vice versa for the active rectifier is:

$$\begin{bmatrix} \alpha \\ \beta \end{bmatrix} = \begin{bmatrix} \frac{2}{3} & -\frac{1}{3} & -\frac{1}{3} \\ 0 & \frac{1}{\sqrt{3}} & -\frac{1}{\sqrt{3}} \end{bmatrix} \begin{bmatrix} a \\ b \\ c \end{bmatrix}$$

$$\begin{bmatrix} a \\ b \\ c \end{bmatrix} = \begin{bmatrix} 1 & 0 \\ -\frac{1}{2} & \frac{\sqrt{3}}{2} \\ -\frac{1}{2} & -\frac{\sqrt{3}}{2} \end{bmatrix} \begin{bmatrix} \alpha \\ \beta \end{bmatrix}$$

Applying this transformation, the voltage equations in  $\alpha\beta$ -coordinates:

$$\begin{bmatrix} u_\alpha \\ u_\beta \end{bmatrix} = R \begin{bmatrix} i_\alpha \\ i_\beta \end{bmatrix} + L \frac{d}{dt} \begin{bmatrix} i_\alpha \\ i_\beta \end{bmatrix} + \begin{bmatrix} u_{S\alpha} \\ u_{S\beta} \end{bmatrix} \quad (2.25 - 2.26)$$

$$C \frac{du_{dc}}{dt} = \frac{3}{2} (S_\alpha i_\alpha + S_\beta i_\beta) - i_{load} \quad (2.27)$$

The active rectifier voltage equations expressed in dq-coordinates is:

$$v_{dq} = v^s e^{-j\theta} \quad (2.28)$$

where,  $v^s = v_\alpha + jv_\beta$ . For the whole equation the following expression can be derived in the dq-system:

$$u^s = Ri^s + L \frac{di^s}{dt} + u_s^s \quad (2.29)$$

$$u_{dq} e^{j\theta} = Ri_{dq} e^{j\theta} + L \left( e^{j\theta} \left( j\omega i_{dq} + \frac{di_{dq}}{dt} \right) \right) + e^{j\theta} u_{sdq} \quad (2.30)$$

Separating real and imaginary part, we obtain

$$u_d = Ri_d + L \frac{di_d}{dt} - \omega Li_q + u_{sd}, \quad (2.31)$$

$$u_q = Ri_q + L \frac{di_q}{dt} + \omega Li_d + u_{sq} \text{ and} \quad (2.32)$$

$$C \frac{du_{dc}}{dt} = \frac{3}{2} (S_d i_d + S_q i_q) - i_{load}. \quad (2.33)$$

The instantaneous power can be determined by transforming from the dq-system to the three-phase system.

We know that for three-phase system

$$P = \text{Re}\{v^s(i^s)^*\} \quad (2.34)$$

$$P = \text{Re}\{v^{dq}(i^{dq})^*\} \quad (2.35)$$

$$v^s(i^s)^* = \left(\frac{2}{3}K\right)^2 \left(v_a(t) + v_b(t)e^{j\frac{2\pi}{3}} + v_c(t)e^{j\frac{4\pi}{3}}\right) \left(i_a(t) + i_b(t)e^{j\frac{2\pi}{3}} + i_c(t)e^{j\frac{4\pi}{3}}\right)^*$$

$$v^s(i^s)^* = \left(\frac{2}{3}K\right)^2 \left[v_a i_a + v_b i_b + v_c i_c + j \frac{1}{\sqrt{3}}(v_a(i_c - i_b) + v_b(i_a - i_c) + v_c(i_b - i_a))\right]$$

The real part gives the active power (P),

$$P = \frac{3}{2K^2} \text{Re}\{v^s(i^s)^*\} \quad (2.36)$$

and moreover,

$$P = \frac{3}{2K^2} \text{Re}\{v^{dq}(i^{dq})^*\}. \quad (2.37)$$

Finally,

$$P = v_a i_a + v_b i_b + v_c i_c. \quad (2.38)$$

And the imaginary part gives the reactive power (Q):

$$Q = \frac{3}{2K^2} \text{Im}\{v^s(i^s)^*\} \quad (2.39)$$

$$Q = \frac{3}{2K^2} \text{Im}\{v^{dq}(i^{dq})^*\} \quad (2.40)$$

$$Q = \frac{1}{\sqrt{3}} [v_a(i_c - i_b) + v_b(i_a - i_c) + v_c(i_b - i_a)] \quad (2.41)$$

So, the active power will be:

$$P = \frac{3}{2K^2} \text{Re}\{v^s(i^s)^*\} \quad (2.42)$$

$$P = \frac{3}{2K^2} \text{Re}\{v^{dq}(i^{dq})^*\} \quad (2.43)$$

$$P = \frac{3}{2} E_m I_m \cos\varphi \quad (2.44)$$

$$P = 3VI\cos\varphi \quad (2.45)$$

DC-Link voltage:

If we want to have low-frequency-harmonic-free current waveforms, a minimum dc-link voltage is needed. The theoretical value of the maximum dc output voltage for a diode rectifier is the peak value of line-to-line RMS voltage. In order to have full control of the converter the diodes must be polarized negatively at all values for the ac-voltage supply. And to keep the diodes blocked we need a dc-link voltage higher than the peak dc-voltage generated by the diodes alone. So we have:

$$V_{DCmin} > \sqrt{2}V_{LL(RMS)} \quad (2.46)$$

$$V_{DCmin} = \sqrt{2}\sqrt{3}V_{LN(RMS)} \quad (2.47)$$

In order to always maintain full control, a DC-link voltage between 15-20% more than  $\sqrt{2}V_{LL}$  is needed.

The DC-link voltage depends on the PWM method. In this case, we will use sinusoidal PWM. Therefore, the maximum reference voltage is  $V_{DC}/2$ .

Finally, the minimum DC-link voltage is:

$$V_{LN(peak)} = \frac{V_{DC}}{2} \quad (2.48)$$

$$\frac{V_{LL(RMS)}}{\sqrt{3}} \sqrt{2} = \frac{V_{DC}}{2} \quad (2.49)$$

$$V_{DC} > 2V_{LN(peak)} \quad (2.50)$$

$$V_{DC} > 2 \frac{\sqrt{2}}{\sqrt{3}} V_{LL(RMS)} \quad (2.51)$$

$$V_{DC} > 1.633 V_{LL(RMS)} \quad (2.52)$$

## 2.1.2 IGBT fundamentals

The IGBT (Insulated Gate Bipolar Transistor) is a three-terminal power semiconductor switch used to control the flow of electrical energy. It is a voltage controlled hybrid switch that combines the characteristics of the BJT and the MOSFET. In figure 2.2 the circuit symbol of the IGBT is shown.

The main advantages of the IGBT over the MOSFET and the BJT are [17]:

- It has a very low on-state voltage drop due to conductivity modulation and has high on-state current density. So, a smaller chip size is possible and the cost can be reduced.
- Low driving power and a simple drive circuit due to the input MOS gate structure. It can be easily controlled as compared to current controlled devices (thyristor, BJT) in high voltage and high current applications.
- Wide SOA. It has a high current conduction capability compared with the bipolar transistor. It has also good forward and reverse blocking capabilities.

The main drawbacks are:

- The switching speed is inferior to MOSFET although superior to BJT. The collector current tailing due to the minority carrier causes the turn-off speed to be slow.
- There is a possibility of latchup due to the internal PNP thyristor structure. This internal parasitic thyristor should not be turn-on because is difficult to turn it off then.

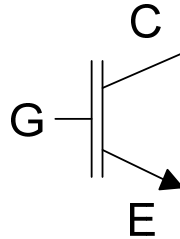


Figure 2.2: Circuit Symbol of IGBT.

So, the BJT has low conduction losses, but switches slowly, whereas the MOSFET switches fast but has high on-state conduction losses [18]. Therefore they were combined to improve the characteristics of the device.

The IGBT looks almost like a MOSFET with drain, source and gate connections. The only difference from a MOSFET in the structure is one more layer to form the drain of the IGBT. In order to understand better, the architecture of the IGBT, in figure 2.3, its basic structure is shown.

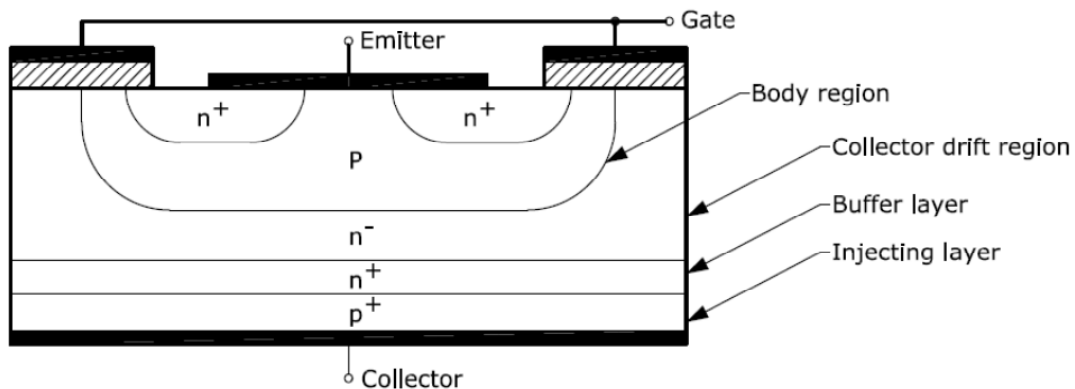


Figure 2.3: Basic Structure of IGBT.

Even though, the IGBT has a physical similarity to the MOSFET, its operation is closer to the BJT. For instance, the presence of the  $p^+$  drain layer (injecting layer) which is responsible for the minority carrier injection into the  $n^-$  drift region and resulting conductivity modulation.

The IGBTs that are manufactured without the buffer layer ( $n^+$  layer) are called NPT (non-punch through IGBTs) whereas those with this layer are called PT (punched through) IGBTs.

This extra buffer layer performs two functions:

a) Avoids failure by punch-through action because the depletion region expansion at applied high voltage is restricted by this layer and

b) Reduces the tail current during turn-off and shortens the fall time of the IGBT.

The NPT IGBTs, which have equal forward and reverse breakdown voltage, are suitable for AC applications. The PT IGBTs, which have less reverse breakdown voltage than the forward breakdown voltage, are applicable for DC circuits where devices are not required to support voltage in the reverse direction. In Table 2.1 the characteristics of both NPT and PT IGBTs are compared.

**Table 2.1:** Comparison of NPT and PT IGBTs:

	NPT	PT
Switching Loss	<b>Medium</b> Long, low amplitude tail current. Moderate increase in $E_{off}$ with temperature	<b>Low</b> Short tail current Significant increase in $E_{off}$ with temperature
Conduction Loss	<b>Medium</b> Increases with temperature	<b>Low</b> Flat to slight decrease with temperature
Paralleling	<b>Easy</b> Optional sorting Recommend share heat	<b>Difficult</b> Must sort on $V_{CE(ON)}$
Short-Circuit Rated	Yes	Limited High gain

### Operation of IGBT

To control the IGBT, a voltage  $V_{GE}$  is applied over gate and emitter. This voltage has to be higher than the threshold voltage  $V_{GE(th)}$  to turn the IGBT on. Figures 2.4 and 2.5 show the turn-on and turn-off waveforms of the IGBT respectively [19].

If the  $V_{GE}$  is below the threshold voltage, the IGBT will be off. If  $V_{GE}$  is higher than the threshold voltage, the IGBT turns on and an inversion layer or channel will be build up beneath the gate. This layer shorts the  $n^-$  drift region to the  $n^+$  source region. The electrons from the source will then flow into the drift region and attract holes from the  $p^+$  drain layer. The holes will then move into the drift region and further into the body region.

When the holes are in the body region they attract electrons from the emitter and recombine. The holes from the  $p^+$  layer will flow directly to the source metallization or to the inversion layer. This results in many holes flowing laterally through the body region. By doing that a resistance is created and this resistance causes a lateral voltage drop. This lateral voltage drop causes the  $n^+ - p$  junction to be forward biased and the parasitic thyristor will be turned on. Therefore, there are always given a maximum collector current and a maximum  $V_{GE}$  from the manufacturers to avoid this latchup. Latchup can also occur during turn-on and turn-off of the device.

Even though the IGBT is in conduction mode, there will always be a voltage drop. The on-state collector-emitter voltage drop  $V_{CE(ON)}$  will be the sum of the voltage drop over the  $p^+ - n^+$ , the voltage drop due to the resistance in the drift region and the voltage drop due to the resistance in the channel:

$$V_{CE(ON)} = V_{junc} + V_{drift} + I_C R_{channel} \quad (2.53)$$

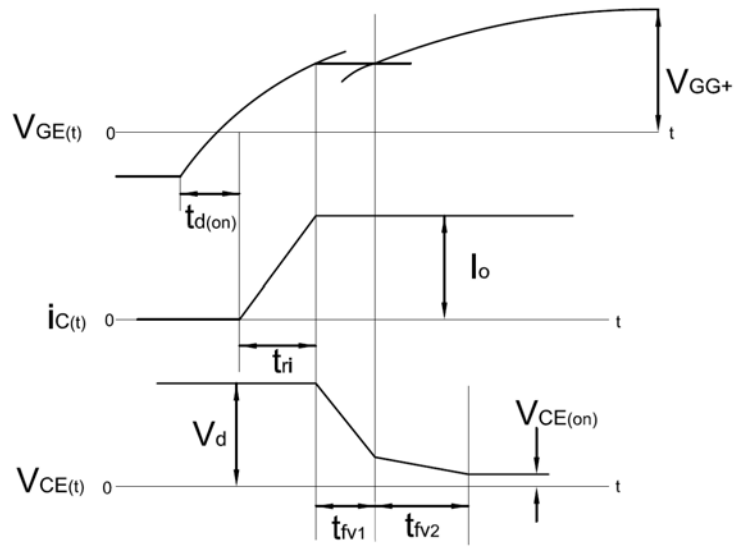


**Figure 2.4:** Turn-on voltage and current waveforms of IGBT.

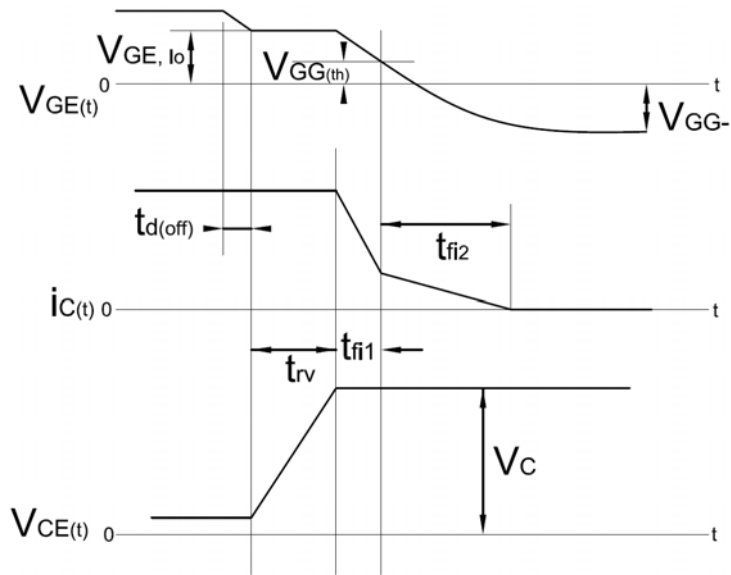


**Figure 2.5:** Turn-off voltage and current waveforms of IGBT.

## 2.2 Modeling of Permanent Magnet Synchronous Machine (PMSG)

### 2.2.1 Introduction and Definition

Permanent magnet synchronous motors have attracted increasing interest in recent years for industrial drive application [20]. The high efficiency, high torque density and simple controllability compared to induction machines, make them a good alternative in main applications [21]. Moreover, the availability of low-cost power electronic devices and the improvement of PM characteristics enable the use of PM motors even in some more high demand applications like wind turbines.

The Permanent Magnet Synchronous Machine is a polyphase AC motor with rotor mounted permanent magnets and sinusoidal distribution of the stator phase windings [22]. The permanent magnets provide the field excitation in the machine instead of the field windings.

By having the magnets on the rotor, the electrical losses of the machine are reduced and the absence of mechanical components such as slip rings and brushes make the machine lighter.

So, the PM motors are basically synchronous machines that can be operated at unity power factor, thus making them more efficient than induction motors. Although they are more expensive than induction machines due to cost of the magnet, but due to its high efficiency the running cost is smaller.

The stator current of an induction motor contains magnetizing as well as torque-producing components. The use of the permanent magnet in the rotor makes it unnecessary to supply magnetizing current through the stator for constant air-gap flux; the stator current needs only to be torque-producing. Therefore, for the same output, the PMSM will operate at a higher power factor and it will be more efficient than the induction machine.

In contrast to the EMSM, the PMSM removed the field coil, dc power supply, and slip rings with permanent magnets. The PMSM, therefore, has a sinusoidal induced EMF and requires sinusoidal currents to produce constant torque. Compared to the EMSM and the induction machine, the PMSM has a higher-torque-to-inertia ratio and power density. In the following diagram, the classification of permanent magnet machines [23] is shown:

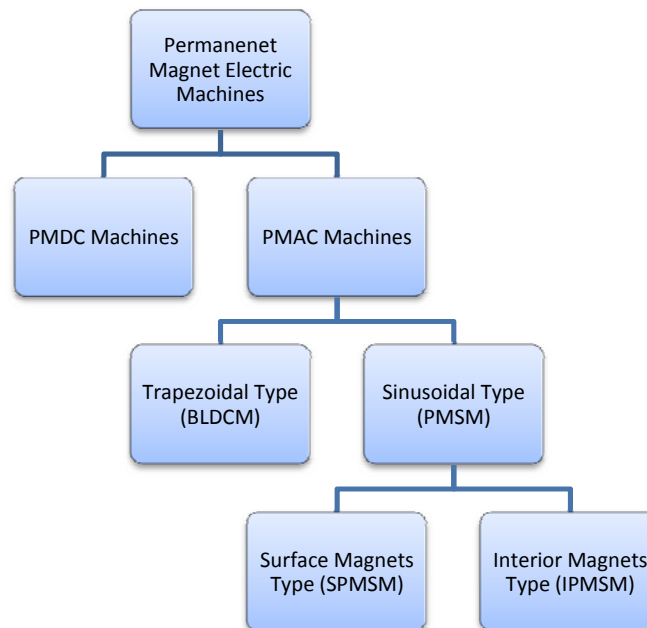


**Figure 2.3:** Classification of Permanent Magnets Machines.

The PMSM or sinusoidal PMAC machine has distributed windings on the stator to provide sinusoidal distribution of field. Also, it has salient pole structure in the rotor, whereas the trapezoidal PMAC machine has non salient structure.

However, the PMSM has some disadvantages: At high temperature or at powerful magnetic fields inside a generator, the permanent magnets are demagnetized (although this is rarely a problem today); difficulties to handle in manufacture and high cost of permanent magnet material.

Since this master thesis' scope is open-loop control, some closed-loop control works of PMSG for wind turbines can be found in [23], [24] and [25].

## 2.2.2 Mathematical Model

The PMSM model equations in the  $\alpha$ - $\beta$  system are [26]:

$$\underline{u}_s^s = R_s \underline{i}_s^s + \frac{d\underline{\psi}_s^s}{dt} \quad (2.54)$$

$$\underline{\psi}_s^s = L_s \lambda \underline{i}_s^s + L_m \underline{i}_s^s + \psi_m e^{j\phi_r} \quad (2.55)$$

$$\underline{\psi}_s^s = L_s \underline{i}_s^s + \psi_m e^{j\phi_r} \quad (2.56)$$

$$\frac{d\underline{\psi}_s^s}{dt} = L_s \frac{d\underline{i}_s^s}{dt} + j\omega_r \psi_m e^{j\phi_r} \quad (2.57)$$

$$\underline{u}_s^s = R_s \underline{i}_s^s + L_s \frac{d\underline{i}_s^s}{dt} + j\omega_r \psi_m e^{j\phi_r} \quad (2.58)$$

$$T_e = \frac{3n_p}{2} \text{Im} \{ \underline{\psi}_s^{s*} \underline{i}_s^s \} \quad (2.59)$$

$$T_e = \frac{3n_p}{2} \text{Im} \{ (L_s \underline{i}_s^s + \psi_m e^{j\phi_r})^* \underline{i}_s^s \} \quad (2.60)$$

$$T_e = \frac{3n_p}{2} \psi_m i_s (\cos \phi_r \sin \theta_s - \sin \phi_r \cos \theta_s) \quad (2.61)$$

$$T_e = \frac{3n_p}{2} \psi_m i_s \sin(\theta_s - \phi_r) \quad (2.62)$$

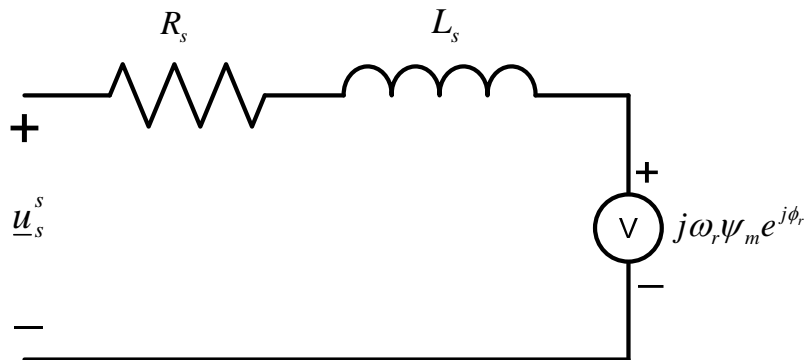


Figure 2.4: Equivalent circuit of PMSM.

$$\underline{u}_s^s = R_s \underline{i}_s^s + L_s \frac{d\underline{i}_s^s}{dt} + j\omega_r \psi_m e^{j\phi_r} \quad (2.63)$$

Splitting into component form:

$$u_{s\alpha} = R_s i_{s\alpha} + L_s \frac{di_{s\alpha}}{dt} - \omega_r \psi_m \sin \phi_r \quad (2.64)$$

$$u_{s\beta} = R_s i_{s\beta} + L_s \frac{di_{s\beta}}{dt} + \omega_r \psi_m \cos \phi_r \quad (2.65)$$

$$T_e = \frac{3n_p}{2} \psi_m (i_{s\beta} \cos \phi_r - i_{s\alpha} \sin \phi_r) \quad (2.66)$$

$$\frac{J}{n_p} \frac{d\omega_r}{dt} = T_e - T_l \quad (2.67)$$

$$\frac{d\phi_r}{dt} = \omega_r \quad (2.68)$$

PMSM Modeling in d-q system:

$$\underline{u}_s^s = R_s \underline{i}_s^s + L_s \frac{d\underline{i}_s^s}{dt} + j\omega_r \psi_m e^{j\phi_r} \quad (2.69)$$

$$\underline{i}_s^s = \underline{i}_s e^{j\theta_r} \quad (2.70)$$

$$\underline{u}_s^s = \underline{u}_s e^{j\theta_r} \quad (2.71)$$

$$\underline{u}_s^s e^{j\theta_r} = R_s \underline{i}_s^s e^{j\theta_r} + L_s \frac{d\underline{i}_s^s}{dt} e^{j\theta_r} + j\omega_r \psi_m e^{j\phi_r} \quad \div e^{j\theta_r}$$

$$\underline{u}_s = R_s \underline{i}_s + L_s \frac{d\underline{i}_s}{dt} + j\omega_r \psi_m e^{j(\phi_r - \theta_r)} \quad (2.72)$$

In component form with perfect field orientation,  $\phi_r = \theta_r$

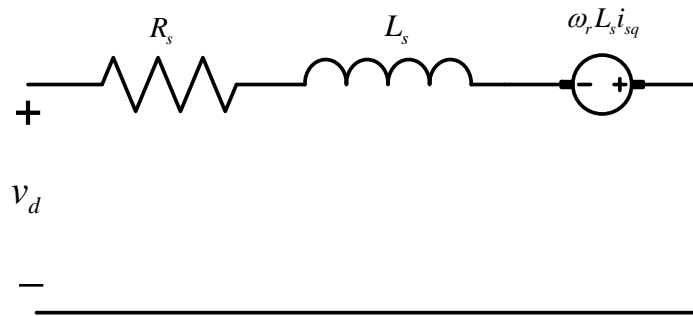


**Figure 2.5:** Equivalent circuit of PMSM in d-axis.

$$u_{sd} = R_s i_{sd} + L_s \frac{di_{sd}}{dt} - \omega_r L_s i_{sq} \quad (2.73)$$

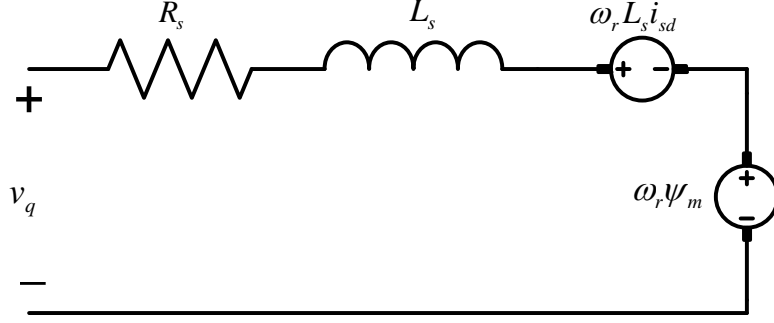


**Figure 2.6:** Equivalent circuit of PMSM in q-axis.

$$u_{sq} = R_s i_{sq} + L_s \frac{di_{sq}}{dt} + \omega_r L_s i_{sd} + \omega_r \psi_m \quad (2.74)$$

$$T_e = \frac{3n_p}{2} \text{Im} \{ \underline{\psi}_s^* \underline{i}_s \} = \frac{3n_p}{2} \text{Im} \{ (L_s \underline{i}_s + \psi_m e^{j\phi_r})^* \underline{i}_s \}$$

$$T_e = \frac{3n_p}{2} \text{Im} \{ (L_{sd} i_{sd} - jL_{sq} i_{sq})(i_{sd} + j i_{sq}) + \psi_m \underline{i}_s \} \quad (2.75)$$

$$T_e = \frac{3n_p}{2} \{ (L_{sd} - L_{sq})(i_{sd} i_{sq}) + \psi_m i_{sq} \} \quad (2.76)$$

$$\frac{J}{n_p} \frac{d\omega_r}{dt} = T_e - T_l$$

$$\frac{d\phi_r}{dt} = \frac{d\theta_r}{dt} = \omega_r$$

### 2.2.3 Machine Design Model

Synchronous motors operate at a constant speed in absolute synchronism with the line frequency [27]. Synchronous motors are classified according to their rotor's design, construction, materials and operation into the four basic groups:

- Electromagnetically-excited motors
- PM motors
- Reluctance motors
- Hysteresis motors

PM synchronous motors can be built with different rotor configurations:

- Classical
- Interior mounted type
- Surfaced mounted type
- Inset-magnet rotor
- Rotor with buried magnets symmetrically distributed
- Rotor with buried magnets asymmetrically distributed

The interior mounted type machine has a smaller effective air gap compared to surface mounted type, and has stronger armature reaction effect.

In our case the generator is a surfaced mounted type (SPMSG): In this case the magnets are mounted on the surface of the outer periphery of rotor laminations [25]. This arrangement provides highest air gap flux density but lacks mechanical robustness. The magnets are magnetized radially. From a magnetic flux path point of view, the magnets can be regarded as

air because the permeability of the magnets is close to unity and the saliency is not present as a consequence of the same width of the magnets. This results that the inductances expressed in the quadrature coordinates are equal,  $L_d = L_q$ .

Good designs require the optimum use of material by operating the motor at highest energy density. The type of magnet used in our Permanent magnet synchronous generator is Neodymium-Boron-Iron 30 (NdFe30) which is a material that has properties equivalent to Samarium-Cobalt with low material cost.



### 3 Case Set-Up

#### 3.1 Case Specification for Permanent Magnet Synchronous Generator

The Permanent Magnet Synchronous Generator that is used in this project is based on a design made in MAXWELL 14.0. The Tables 3.1, 3.2 and 3.3 show the most important data of the generator that was taken from the MAXWELL design:

**Table 3.1:** General Data of PMSG

Rated Output Power	4.1 MW
Rated Voltage	10 kV
Number of Poles	4
Frequency	50 Hz
Operating Temperature	75°C

**Table 3.2:** Steady State Parameters of PMSG

D-Axis Reactance	12.082 ohm
Q-Axis Reactance	12.082 ohm
Armature Phase Resistance	0.056 ohm

**Table 3.3:** Full-load Data of PMSG

RMS Line Current	313.011 A
RMS Phase Current	313.011 A
RMS Phase Voltage	5773.5
Total Loss	54755.2 W
Efficiency	98.92%
Power Factor	0.9224
Synchronous Speed	1500 rpm
Rated Torque	32183.4 N.m
Fundamental Induced RMS Line Voltage	9378.02 V

#### 3.2 Active Rectifier Circuit Diagram for PMSG

An overview of the wind turbine, the permanent magnet synchronous generator and the active rectifier circuit diagram can be seen in Figure 3.1. The figure shows basically the scope of this project. For each phase leg, there will be IGBTs put in series in order to fulfill the voltage requirement, since a single IGBT cannot withstand the phase voltage level of the output of the generator. Therefore, IGBTs ABB HiPak will be used in the design of the converter.

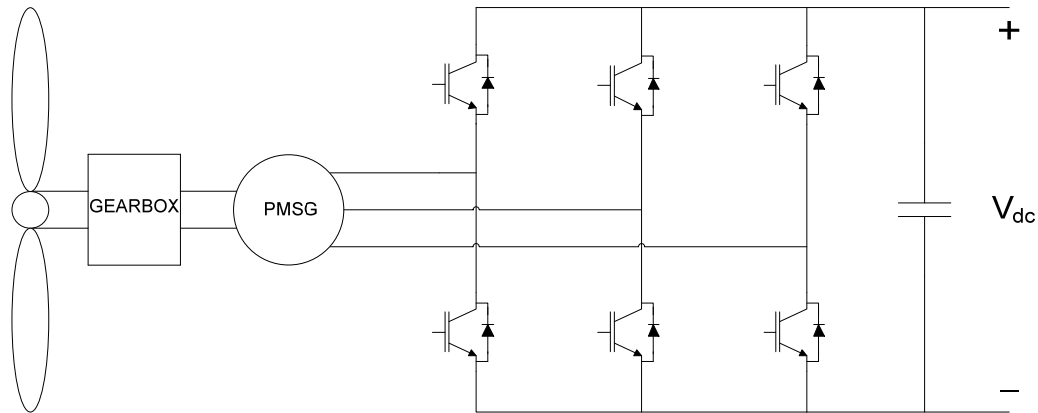


**Figure 3.1:** Active rectifier circuit diagram used with the PMSG for the offshore wind turbine.

### 3.3 Specification of the Power Electronic System (IGBT's Specification)

As it was mentioned in section 3.2, HiPak IGBT modules were chosen for the power electronic system that will be implemented, which in our case is the active rectifier. All the datasheets are available at [www.abb.com/semiconductors](http://www.abb.com/semiconductors). The main reasons for choosing HiPak family of IGBT modules were that they combine low-losses with soft-switching performance and record-breaking Safe Operating Area (SOA). Also the HiPak family sets new standards of robustness for high reliability applications. Robustness translates to higher operating safety margins and allows low gate drive resistance at turn-off, which in turn, allows lower turn-off losses.

Three different voltage levels are used: 3.3 kV, 4.5 kV and 6.5 kV. And the base temperature that was used was 125°C. In figures 3.2, 3.3, 3.4 and 3.5, the different datasheets for the ABB HiPak 3.3 kV module are shown and after each figure, the calculation of the parameters is shown. The process was repeated for the 4.5 kV and 6.5 kV modules. Table 3.4 shows the summary of the parameters of the 3 different modules used.

### ABB HiPak 3.3 kV Module datasheets and parameter calculations:

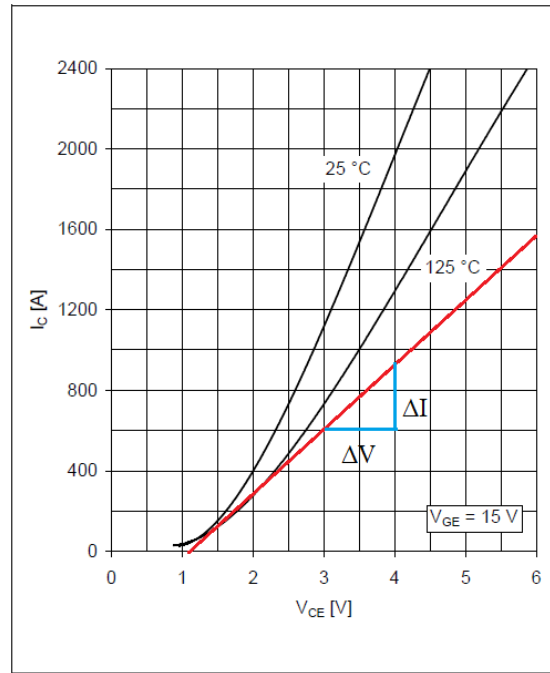


**Figure 3.2:** Typical on-state characteristics of IGBT for 3.3 kV ABB HiPak module.

From Figure 3.2, two important parameters are known: The on-state collector-emitter voltage drop  $V_{CE(ON)}$  and the on-state resistance of the IGBT,  $R_{CE(ON)}$ .

From the figure above, an approximation has been made in order to get the parameters since our operating point of current is 600A. Therefore,  $V_{CE(ON)}=1.1\text{V}$  and the  $R_{CE(ON)}=\Delta V/\Delta I$  which is equal to 3.33 m $\Omega$ .

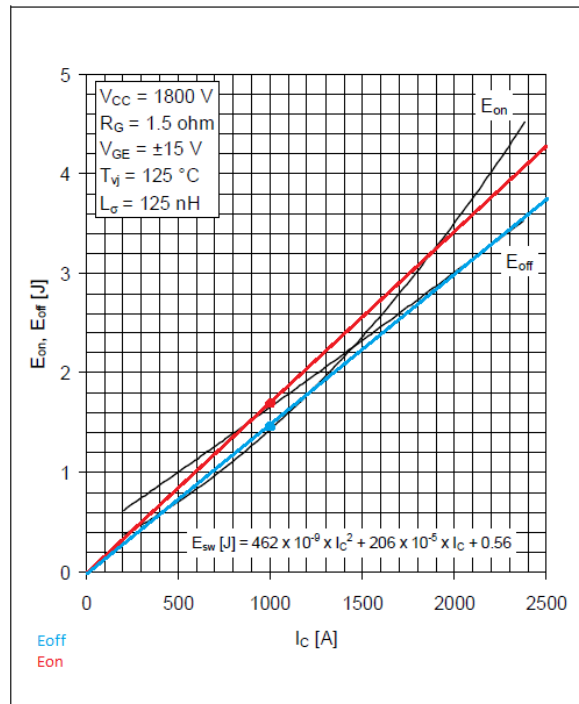


**Figure 3.3:** Typical switching energies per pulse vs. collector current for 3.3 kV ABB HiPak module.

From figure 3.3, the switching energy at the turn-on ( $E_{SW\_IGBT(ON)}$ ) and the switching energy at the turn-off  $E_{SW\_IGBT(OFF)}$  of the IGBT can be taken. For this case,  
 $E_{SW\_IGBT(ON)}=0.00165$  Joules/A.  
 $E_{SW\_IGBT(OFF)}=0.00145$  Joules/A.

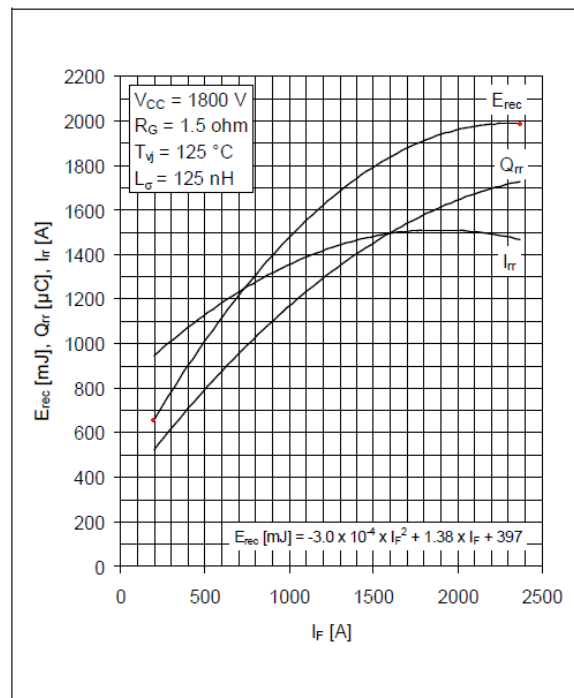


**Figure 3.4:** Typical reverse recovery characteristics vs. forward current of freewheeling diode for the 3.3 kV ABB HiPak module.

From figure 3.4, the reverse recovery energy of the diode  $E_{rec}$  can be taken. The calculation for this parameter consists in taking two points from the graph and then finding an exponent for it which we will call  $K_i D$ . A linear approximation is not possible because the results would not be accurate enough. Therefore, the calculation is as follows:

Point 1: (200, 0.675). Point 2: (2370, 1.98)

$$\left(\frac{x_2}{x_1}\right)^{K_i D} = \frac{y_2}{y_1}$$

$$\left(\frac{2370}{200}\right)^{K_i D} = \frac{1.98}{0.675}$$

$$(11.85)^{K_i D} = 2.93$$

$$K_i D \ln 11.85 = \ln 2.93$$

$$K_i D = 0.435$$

Since our rated current reference is 1A, the reverse recovery energy  $E_{rec}$  is equal to,

$$E_{rec} = 0.675 \left(\frac{1}{200}\right)^{0.435} = 0.067 \text{ Joules.}$$

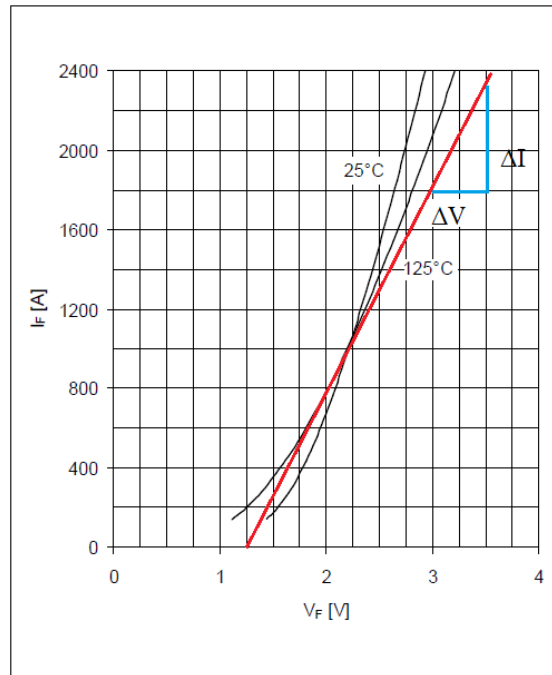


**Figure 3.5:** Typical diode forward characteristics for the 3.3 kV ABB HiPak module.

From figure 3.5, two important parameters are known: The forward voltage  $V_F$  and the on-state resistance of the diode,  $R_F$ .

From the figure,  $V_F=1.2\text{V}$  and the  $R_F=\Delta V/\Delta I$  which is equal to  $0.909 \text{ m}\Omega$ .

The same process was made for the 4.5 kV and the 6.5 kV modules. In Table 3.6, all the parameters are shown for each module:

**Table 3.4:** Parameters of HiPak modules

<b>Parameters</b>	<b>HiPak Modules</b>		
	<b>3.3 kV</b>	<b>4.5 kV</b>	<b>6.5 kV</b>
$V_{ref}$	1800 V	2800 V	3600 V
$I_{ref}$	1 A	1 A	1 A
$V_{CE(ON)}$	1.1 V	1.15 V	1.2 V
$R_{CE(ON)}$	3.33 m $\Omega$	2.5 m $\Omega$	3.6 m $\Omega$
$E_{SW\_IGBT(ON)}$	0.00165 J	0.0044 J	0.0085 J
$E_{SW\_IGBT(OFF)}$	0.00145 J	0.00475 J	0.0072 J
$V_F$	1.2 V	1.55 V	1.5 V
$R_F$	0.909 m $\Omega$	2.083 m $\Omega$	2.6 m $\Omega$
$K_jD$	0.435	0.564	0.579
$E_{rec}$	0.067 J	0.0465 J	0.054 J

From the datasheets shown above, there is important data needed for the loss calculation.

## 4 Analysis (Results and Discussions)

### 4.1 Verification of main operation with MATLAB

The design of the converter is based on the parameters given in Table 4.1 that presents the operation of the permanent magnet synchronous generator at different wind speeds. For each wind speed the mechanical speed, the active power and the electrical torque are shown based on experimental results [28].

**Table 4.1:** Operation of Permanent Magnet Synchronous Generator at different wind speeds.

Wind Speed	Mechanical Speed	Active Power	Electrical Torque
12-25 m/s	1500 rpm	5000 kW	31.83 kN.m
10 m/s	1500 rpm	4080 kW	25.98 kN.m
8 m/s	1479.73 rpm	2100 kW	13.55 kN.m
6 m/s	1155.4 rpm	740 kW	6.12 kN.m
5 m/s	972.97 rpm	374 kW	3.67 kN.m
4 m/s	881.76 rpm	130 kW	1.41 kN.m

We know that the back-emf is equal to the flux multiplied by the electrical speed in rad/s:

$$e = \psi_m \omega_r$$

In Table 3.3 it is shown the value of the line to line back-emf of the generator which is 9378.02 V. Note that the back-emf ( $e$ ) that should be used for amplitude invariant transformation is the peak phase value:

$$e = \frac{9378.02}{\sqrt{3}} \times \sqrt{2} = 7657.12 \text{ V}$$

$$\omega_r = \omega_m \times n_p = 157.08 \times 2 = 314.16 \text{ rad/s}$$

$$\psi_m = \frac{e}{\omega_r} = \frac{7657.12}{314.16} = 24.37 \text{ Wb}$$

Case 1: Wind Speed=12-25 m/s.  $P = 5000 \text{ kW}$ .  $T_e = 31.83 \text{ kN.m}$ .  $\psi_m = 24.37 \text{ Wb}$ .

$$\omega_r = 314.16 \text{ rad/s.}$$

$$f = \frac{\omega_r}{2\pi} = \frac{314.16}{2\pi} = 50 \text{ Hz}$$

$$T_e = \frac{3n_p}{2} \{ (L_{sd} - L_{sq})(i_{sd}i_{sq}) + \psi_m i_{sq} \}$$

Since it is a non-salient machine  $L_{sd} = L_{sq}$ . Therefore, the formula simplifies to:

$$T_e = \frac{3n_p}{2} (\psi_m i_{sq})$$

Now we calculate the current:

$$i_{sq} = T_e \frac{2}{3n_p \psi_m} = 31830 \left( \frac{2}{3 \times 2 \times 24.37} \right)$$

$$i_{sq} = 435.37 \text{ A (peak value)} \div \sqrt{2}$$

$$\mathbf{i_{sq} = 307.85 \text{ A (RMS value)}}$$

$$i_{sd} = 0 \text{ A}$$

Having the value of the current, we proceed to calculate the voltage of the converter using (2.73) to calculate the voltage in the d-direction:

$$u_{sd} = R_s i_{sd} + L_s \frac{di_{sd}}{dt} - \omega_r L_s i_{sq}$$

$$u_{sd} = 0 + 0 - (314.16 \times 0.03846 \times 435.37) = -5260.4 \text{ V}$$

Now we use (2.74) to calculate the voltage in the q-direction:

$$u_{sq} = R_s i_{sq} + L_s \frac{di_{sq}}{dt} + \omega_r L_s i_{sd} + \omega_r \psi_m$$

$$u_{sq} = (0.056 \times 435.37) + 0 + 0 + (314.16 \times 24.37) = 7680.46 \text{ V}$$

$$U_{converter(dq)} = -5260.4 + j7680.46 \text{ V (peak-phase value)}$$

$$U_{converter(dq)} = -6442.16 + j9406.6 \text{ V (line-line RMS value)}$$

$$|U_{converter(dq)}| = 11401.12 \text{ V (line-line RMS)}$$

$$U_{converter,a} = 6582.44 \angle -34.41^\circ \text{ V (phase-RMS value)}$$

$$U_{converter,b} = 6582.44 \angle -154.41^\circ \text{ V (phase-RMS value)}$$

$$U_{converter,c} = 6582.44 \angle 85.59^\circ \text{ V (phase-RMS value)}$$

This calculation is the same for the other 5 cases. In Table 4.2, a summary of the data needed for the operation of the converter is shown:

**Table 4.2:** Calculated data needed for the operation of the active rectifier.

Wind Speed	Generator Speed	Frequency	Reactance	Back-Emf (peak-phase)	Current (RMS)
12-25 m/s	157.08 rad/s	50.00 Hz	12.082 $\Omega$	7657.12 V	307.85 A
10 m/s	157.08 rad/s	50.00 Hz	12.082 $\Omega$	7657.12 V	251.25 A
8 m/s	154.96 rad/s	49.32 Hz	11.92 $\Omega$	7552.75 V	131.05 A
6 m/s	121 rad/s	38.51 Hz	9.306 $\Omega$	5897.05 V	59.19 A
5 m/s	102.62 rad/s	32.43 Hz	7.84 $\Omega$	4966.12 V	35.50 A
4 m/s	92.34 rad/s	29.39 Hz	7.102 $\Omega$	4500.65 V	13.64 A

The dc-link voltage ( $V_{dc}$ ) that was chosen was 16467 V. In Section 2.1.1 (Active rectifier definition) the process of calculating and choosing the output dc voltage is explained and finally by using (2.52) we reach the desired value of the dc voltage.

Then, because of the voltage level that we are working with, the IGBTs should be put in series and in parallel in order to fulfill the voltage and current levels respectively taking into account an overvoltage factor. In our case the overvoltage factor (OV) that was chosen was 1.55.

The calculation of the number of series modules and parallel modules for each position in the converter is as following:

$$\text{series modules} = \text{ceil} \left( \frac{V_{dc}}{2} \cdot \frac{OV}{V_{ref}} \right) \quad (4.1)$$

$$\text{parallel modules} = \text{ceil} \left( \frac{I_{rms}}{I_{rms\_rated}} \right) \quad (4.2)$$

$I_{rms\_rated}$  is the rated that current that the IGBT can withstand. From datasheets is the value of  $I_c$  divided by 2. For example for the 3.3 kV module the  $I_{rms\_rated} = \frac{1200}{2} = 600$  A.

In table 4.3 the number of modules in series and in parallel is shown for each HiPak module:

**Table 4.3:** Number of modules in series and in parallel used in the converter (for each position and total).

HiPak Module	Number of series modules	Number of parallel modules	Total Modules
3.3 kV	8	1	48
4.5 kV	5	1	30
6.5 kV	4	1	24

The technique used to switch on and off the IGBTs was Pulse Width Modulation (PWM). It was simply made by comparing a triangular wave with a sinusoidal waveform. The operating principle can be seen in figure 4.1.

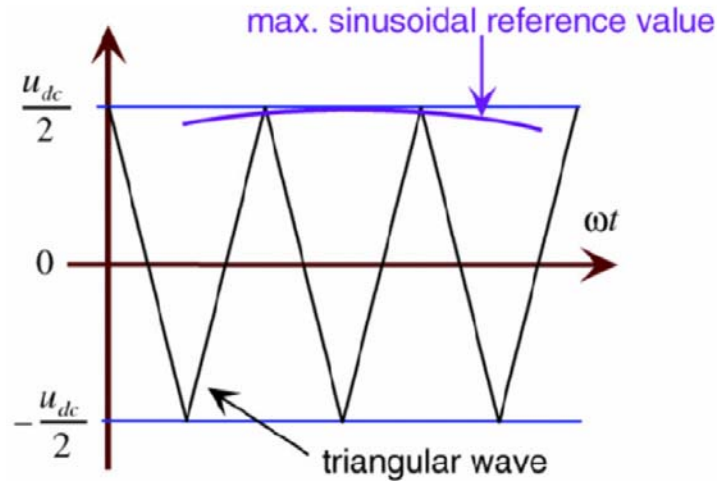


**Figure 4.1:** PWM used to switch on and off the IGBTs.

## 4.2 Calculation of Losses as function of Switching Frequency

For the loss calculation of the active rectifier, SEMIKRON formulas [29] were used. The switching losses formulas are:

For the IGBT:

$$P_{sw\_IGBT} = f_{sw} E_{sw} \left( \frac{1 \hat{I}_{out}}{\pi I_{ref}} \right)^{K_i IGBT} \left( \frac{V_{cc}}{V_{ref}} \right)^{K_v IGBT} \quad (4.3)$$

where the constant  $K_i IGBT \approx 1$  and the constant  $K_v IGBT \approx 1.35$

Moreover  $E_{sw}$  is the sum of  $E_{sw\_IGBT(ON)}$  and  $E_{sw\_IGBT(OFF)}$

The current  $\hat{I}_{out}$  is the peak value of the RMS current shown in Table 4.2 and  $V_{cc}$  is the voltage taken by each IGBT after putting all the modules in series. It is calculated in this way:

$$V_{cc} = \frac{V_{dc}}{2(\text{series modules})} \quad (4.4)$$

For the freewheeling diode:

$$P_{sw\_D} = f_{sw} E_{rec} \left( \frac{1 \hat{I}_{out}}{\pi I_{ref}} \right)^{K_i D} \left( \frac{V_{cc}}{V_{ref}} \right)^{K_v D} \quad (4.5)$$

where the constant  $K_i D$  was calculated in Section 3.3 and has different values for each module and the constant  $K_v D \approx 0.6$ .

The conduction losses are:

For the IGBT:

$$P_{cond\_IGBT} = \left( \frac{1}{2\pi} + \frac{M \cos \varphi}{8} \right) V_{CE(ON)} \hat{I}_{out} + \left( \frac{1}{8} + \frac{M \cos \varphi}{3\pi} \right) R_{CE(ON)} (\hat{I}_{out})^2 \quad (4.6)$$

and for the freewheeling diode:

$$P_{cond\_D} = \left( \frac{1}{2\pi} - \frac{M \cos \varphi}{8} \right) V_F \hat{I}_{out} + \left( \frac{1}{8} - \frac{M \cos \varphi}{3\pi} \right) R_F (\hat{I}_{out})^2 \quad (4.7)$$

M is the amplitude modulation which in our case is equal to 0.93.

The loss calculation results are shown from Table 4.1 until Table 4.21. In each table, calculations are presented for three different wind speeds. The loss values of the IGBT and the freewheeling diode are shown separately.

Tables 4.19, 4.20 and 4.21 show the total losses for the three-phase converter at full speed and also the efficiency of the converter. Afterwards, some plots are shown and finally the efficiency of the active rectifier for full speed is calculated with each module.

**Table 4.1: Switching Losses (W) with 1 kHz switching frequency for 1 IGBT**

HiPak Module	Wind Speed					
	12-25 m/s		8 m/s		4 m/s	
	IGBT	FWD	IGBT	FWD	IGBT	FWD
<b>3.3 kV</b>	201.98	409.31	85.99	282.30	8.95	105.50
<b>4.5 kV</b>	619.29	545.82	263.64	337.19	27.44	94.12
<b>6.5 kV</b>	1022.95	671.08	435.48	409.29	45.32	110.43
<b>Total 3.3 kV</b>	611.29		368.29		114.45	
<b>Total 4.5 kV</b>	1165.11		600.83		121.56	
<b>Total 6.5 kV</b>	1694.03		844.77		155.75	

**Table 4.2: Switching Losses (W) with 1 kHz switching frequency for 1 position**

HiPak Module	Wind Speed					
	12-25 m/s		8 m/s		4 m/s	
	IGBT	FWD	IGBT	FWD	IGBT	FWD
<b>3.3 kV</b>	1615.87	3274.46	687.89	2258.42	71.59	844.03
<b>4.5 kV</b>	3096.43	2729.09	1318.18	1685.93	137.19	470.58
<b>6.5 kV</b>	4091.79	2684.32	1741.92	1637.16	181.30	441.72
<b>Total 3.3 kV</b>	4890.33		2946.31		915.62	
<b>Total 4.5 kV</b>	5825.52		3004.11		607.77	
<b>Total 6.5 kV</b>	6776.11		3379.08		623.02	

**Table 4.3: Switching Losses (W) with 1 kHz switching frequency for 3 phases (full converter)**

HiPak Module	Wind Speed					
	12-25 m/s		8 m/s		4 m/s	
	IGBT	FWD	IGBT	FWD	IGBT	FWD
<b>3.3 kV</b>	9695.20	19646.74	4127.35	13550.50	429.57	5064.16
<b>4.5 kV</b>	18578.59	16374.55	7909.10	10115.56	823.17	2823.46
<b>6.5 kV</b>	24550.76	16105.90	10451.52	9822.96	1087.78	2650.29
<b>Total 3.3 kV</b>	29341.94		17677.85		5493.73	
<b>Total 4.5 kV</b>	34953.14		18024.66		3646.63	
<b>Total 6.5 kV</b>	40656.66		20274.48		3738.07	

**Table 4.4: Conduction Losses (W) with 1 kHz switching frequency for 1 IGBT**

HiPak Module	Wind Speed					
	12-25 m/s		8 m/s		4 m/s	
	IGBT	FWD	IGBT	FWD	IGBT	FWD
<b>3.3 kV</b>	252.43	40.55	79.87	11.90	5.05	2.13
<b>4.5 kV</b>	225.51	59.89	76.14	16.36	5.22	2.77
<b>6.5 kV</b>	274.10	62.79	86.89	16.47	5.51	2.69
<b>Total 3.3 kV</b>	292.98		91.77		7.18	
<b>Total 4.5 kV</b>	285.4		92.5		7.99	
<b>Total 6.5 kV</b>	336.89		103.36		8.2	

**Table 4.5: Conduction Losses (W) with 1 kHz switching frequency for 1 position**

HiPak Module	Wind Speed					
	12-25 m/s		8 m/s		4 m/s	
	IGBT	FWD	IGBT	FWD	IGBT	FWD
<b>3.3 kV</b>	2019.45	324.43	638.98	95.23	40.42	17.01
<b>4.5 kV</b>	1127.56	299.45	380.70	81.81	26.08	13.84
<b>6.5 kV</b>	1096.40	251.14	347.55	65.87	22.04	10.78
<b>Total 3.3 kV</b>	2343.88		734.21		57.43	
<b>Total 4.5 kV</b>	1427.01		462.51		39.92	
<b>Total 6.5 kV</b>	1347.54		413.42		32.82	

**Table 4.6: Conduction Losses (W) with 1 kHz switching frequency for 3 phases (full converter)**

HiPak Module	Wind Speed					
	12-25 m/s		8 m/s		4 m/s	
	IGBT	FWD	IGBT	FWD	IGBT	FWD
<b>3.3 kV</b>	12124.72	1946.55	3833.87	571.39	242.54	102.04
<b>4.5 kV</b>	6765.33	1796.72	2284.18	490.85	156.47	83.06
<b>6.5 kV</b>	6578.38	1506.85	2085.31	395.22	132.24	64.65
<b>Total 3.3 kV</b>	14071.27		4405.26		344.58	
<b>Total 4.5 kV</b>	8562.05		2775.03		239.53	
<b>Total 6.5 kV</b>	8085.23		2480.53		196.89	

**Table 4.7: Switching Losses (W) with 3.4 kHz switching frequency for 1 IGBT**

HiPak Module	Wind Speed					
	12-25 m/s		8 m/s		4 m/s	
	IGBT	FWD	IGBT	FWD	IGBT	FWD
<b>3.3 kV</b>	686.74	1391.64	292.35	959.83	30.43	358.71
<b>4.5 kV</b>	2105.57	1855.78	896.37	1146.43	93.29	319.99
<b>6.5 kV</b>	3478.02	2281.67	1480.63	1391.59	154.10	375.46
<b>Total 3.3 kV</b>	2078.38		1252.18		389.14	
<b>Total 4.5 kV</b>	3961.35		2042.80		413.28	
<b>Total 6.5 kV</b>	5759.69		2872.22		529.56	

**Table 4.8: Switching Losses (W) with 3.4 kHz switching frequency for 1 position**

HiPak Module	Wind Speed					
	12-25 m/s		8 m/s		4 m/s	
	IGBT	FWD	IGBT	FWD	IGBT	FWD
<b>3.3 kV</b>	5493.95	11133.16	2338.83	7678.62	243.42	2869.69
<b>4.5 kV</b>	10527.87	9278.91	4481.83	5732.15	466.46	1599.96
<b>6.5 kV</b>	13912.10	9126.68	5922.53	5566.34	616.41	1501.83
<b>Total 3.3 kV</b>	16627.11		10017.45		3113.11	
<b>Total 4.5 kV</b>	19806.78		10213.98		2066.42	
<b>Total 6.5 kV</b>	23038.78		11488.87		2118.24	

Table 4.9: Switching Losses (W) with 3.4 kHz switching frequency for 3 phases (full converter)

HiPak Module	Wind Speed					
	12-25 m/s		8 m/s		4 m/s	
	IGBT	FWD	IGBT	FWD	IGBT	FWD
3.3 kV	32963.69	66798.93	14032.99	46071.71	1460.53	17218.14
4.5 kV	63167.22	55673.46	26890.95	34392.90	2798.77	9599.76
6.5 kV	83472.57	54760.06	35535.16	33398.05	3698.44	9011.00
<b>Total 3.3 kV</b>	99762.62		60104.70		18678.67	
<b>Total 4.5 kV</b>	118840.68		61283.85		12398.53	
<b>Total 6.5 kV</b>	138232.63		68933.21		12709.40	

Table 4.10: Conduction Losses (W) with 3.4 kHz switching frequency for 1 IGBT

HiPak Module	Wind Speed					
	12-25 m/s		8 m/s		4 m/s	
	IGBT	FWD	IGBT	FWD	IGBT	FWD
3.3 kV	252.43	40.55	79.87	11.90	5.05	2.13
4.5 kV	225.51	59.89	76.14	16.36	5.22	2.77
6.5 kV	274.10	62.79	86.89	16.47	5.51	2.69
<b>Total 3.3 kV</b>	292.98		91.77		7.18	
<b>Total 4.5 kV</b>	285.4		92.5		7.99	
<b>Total 6.5 kV</b>	336.89		103.36		8.2	

Table 4.11: Conduction Losses (W) with 3.4 kHz switching frequency for 1 position

HiPak Module	Wind Speed					
	12-25 m/s		8 m/s		4 m/s	
	IGBT	FWD	IGBT	FWD	IGBT	FWD
3.3 kV	2019.45	324.43	638.98	95.23	40.42	17.01
4.5 kV	1127.56	299.45	380.70	81.81	26.08	13.84
6.5 kV	1096.40	251.14	347.55	65.87	22.04	10.78
<b>Total 3.3 kV</b>	2343.88		734.21		57.43	
<b>Total 4.5 kV</b>	1427.01		462.51		39.92	
<b>Total 6.5 kV</b>	1347.54		413.42		32.82	

Table 4.12: Conduction Losses (W) with 3.4 kHz switching frequency for 3 phases (full converter)

HiPak Module	Wind Speed					
	12-25 m/s		8 m/s		4 m/s	
	IGBT	FWD	IGBT	FWD	IGBT	FWD
3.3 kV	12116.71	1946.55	3833.87	571.39	242.54	102.04
4.5 kV	6765.33	1796.72	2284.18	490.85	156.47	83.06
6.5 kV	6578.38	1506.85	2085.31	395.22	132.24	64.65
<b>Total 3.3 kV</b>	14063.26		4405.26		344.58	
<b>Total 4.5 kV</b>	8562.05		2775.03		239.53	
<b>Total 6.5 kV</b>	8085.23		2480.53		196.89	

**Table 4.13: Switching Losses (W) with 5 kHz switching frequency for 1 IGBT**

HiPak Module	Wind Speed					
	12-25 m/s		8 m/s		4 m/s	
	IGBT	FWD	IGBT	FWD	IGBT	FWD
<b>3.3 kV</b>	1009.90	2046.50	429.93	1411.50	44.75	527.52
<b>4.5 kV</b>	3096.40	2729.10	1318.20	1685.90	137.19	470.58
<b>6.5 kV</b>	5114.70	3355.40	2177.40	2046.40	226.62	552.14
<b>Total 3.3 kV</b>	3056.40		1841.43		572.27	
<b>Total 4.5 kV</b>	5825.50		3004.10		607.77	
<b>Total 6.5 kV</b>	8470.10		4223.80		778.76	

**Table 4.14: Switching Losses (W) with 5 kHz switching frequency for 1 position**

HiPak Module	Wind Speed					
	12-25 m/s		8 m/s		4 m/s	
	IGBT	FWD	IGBT	FWD	IGBT	FWD
<b>3.3 kV</b>	8079.30	16372.00	3439.50	11292.00	357.97	4220.13
<b>4.5 kV</b>	15482.00	13645.00	6590.90	8429.60	685.97	2352.88
<b>6.5 kV</b>	20459.00	13422.00	8709.60	8185.80	906.48	2208.58
<b>Total 3.3 kV</b>	24451.30		14731.50		4578.10	
<b>Total 4.5 kV</b>	29127.00		15020.50		3038.85	
<b>Total 6.5 kV</b>	33881.00		16895.40		3115.06	

**Table 4.15: Switching Losses (W) with 5 kHz switching frequency for 3 phases (full converter)**

HiPak Module	Wind Speed					
	12-25 m/s		8 m/s		4 m/s	
	IGBT	FWD	IGBT	FWD	IGBT	FWD
<b>3.3 kV</b>	48476.00	98234.00	20637.00	67753.00	2147.84	25320.79
<b>4.5 kV</b>	92893.00	81873.00	39546.00	50578.00	4115.84	14117.29
<b>6.5 kV</b>	122750.00	80529.00	52258.00	49115.00	5438.89	13251.47
<b>Total 3.3 kV</b>	146710.00		88390.00		27468.63	
<b>Total 4.5 kV</b>	174766.00		90124.00		18233.13	
<b>Total 6.5 kV</b>	203279.00		101373.00		18690.36	

**Table 4.16: Conduction Losses (W) with 5 kHz switching frequency for 1 IGBT**

HiPak Module	Wind Speed					
	12-25 m/s		8 m/s		4 m/s	
	IGBT	FWD	IGBT	FWD	IGBT	FWD
<b>3.3 kV</b>	252.43	40.55	79.87	11.90	5.05	2.13
<b>4.5 kV</b>	225.51	59.89	76.14	16.36	5.22	2.77
<b>6.5 kV</b>	274.10	62.79	86.89	16.47	5.51	2.69
<b>Total 3.3 kV</b>	292.98		91.77		7.18	
<b>Total 4.5 kV</b>	285.40		92.5		7.99	
<b>Total 6.5 kV</b>	336.89		103.36		8.2	

**Table 4.17: Conduction Losses (W) with 5 kHz switching frequency for 1 position**

HiPak Module	Wind Speed					
	12-25 m/s		8 m/s		4 m/s	
	IGBT	FWD	IGBT	FWD	IGBT	FWD
<b>3.3 kV</b>	2019.50	324.43	638.98	95.23	40.42	17.01
<b>4.5 kV</b>	1127.60	299.45	380.70	81.81	26.08	13.84
<b>6.5 kV</b>	1096.40	251.14	347.55	65.87	22.04	10.78
<b>Total 3.3 kV</b>	2343.93		734.21		57.43	
<b>Total 4.5 kV</b>	1427.05		462.51		39.92	
<b>Total 6.5 kV</b>	1347.54		413.42		32.82	

**Table 4.18: Conduction Losses (W) with 5 kHz switching frequency for 3 phases (full converter)**

HiPak Module	Wind Speed					
	12-25 m/s		8 m/s		4 m/s	
	IGBT	FWD	IGBT	FWD	IGBT	FWD
<b>3.3 kV</b>	12117.00	1946.60	3833.90	571.39	242.54	102.04
<b>4.5 kV</b>	6765.30	1796.70	2284.20	490.85	156.47	83.06
<b>6.5 kV</b>	6578.40	1506.80	2085.30	395.22	132.24	64.65
<b>Total 3.3 kV</b>	14063.60		4405.29		344.58	
<b>Total 4.5 kV</b>	8562.00		2775.05		239.53	
<b>Total 6.5 kV</b>	8085.20		2480.52		196.89	

**Table 4.19: Total loss (W) with 1 kHz switching frequency for 3 phases (full converter)**

Module	Loss in 1 IGBT		Loss in full converter		Loss percentage
	Switching	Conduction	Switching	Conduction	
<b>3.3 kV</b>	611.29	292.98	29341.94	14071.27	1.053%
<b>4.5 kV</b>	1165.11	285.40	34953.14	8562.05	1.056%
<b>6.5 kV</b>	1694.03	336.89	40656.66	8085.23	1.18%

**Table 4.20: Total loss (W) with 3.4 kHz switching frequency for 3 phases (full converter)**

Module	Loss in 1 IGBT		Loss in full converter		Loss percentage
	Switching	Conduction	Switching	Conduction	
<b>3.3 kV</b>	2078.38	292.98	99762.62	14063.26	2.76%
<b>4.5 kV</b>	3961.35	285.40	118840.68	8562.05	3.09%
<b>6.5 kV</b>	5759.69	336.89	138232.63	8085.23	3.55%

**Table 4.21: Total loss (W) with 5 kHz switching frequency for 3 phases (full converter)**

Module	Loss in 1 IGBT		Loss in full converter		Loss percentage
	Switching	Conduction	Switching	Conduction	
<b>3.3 kV</b>	3056.40	292.98	146710.00	14063.60	3.90%
<b>4.5 kV</b>	5825.50	285.40	174766.00	8562.00	4.45%
<b>6.5 kV</b>	8470.10	336.89	203279.00	8085.20	5.13%

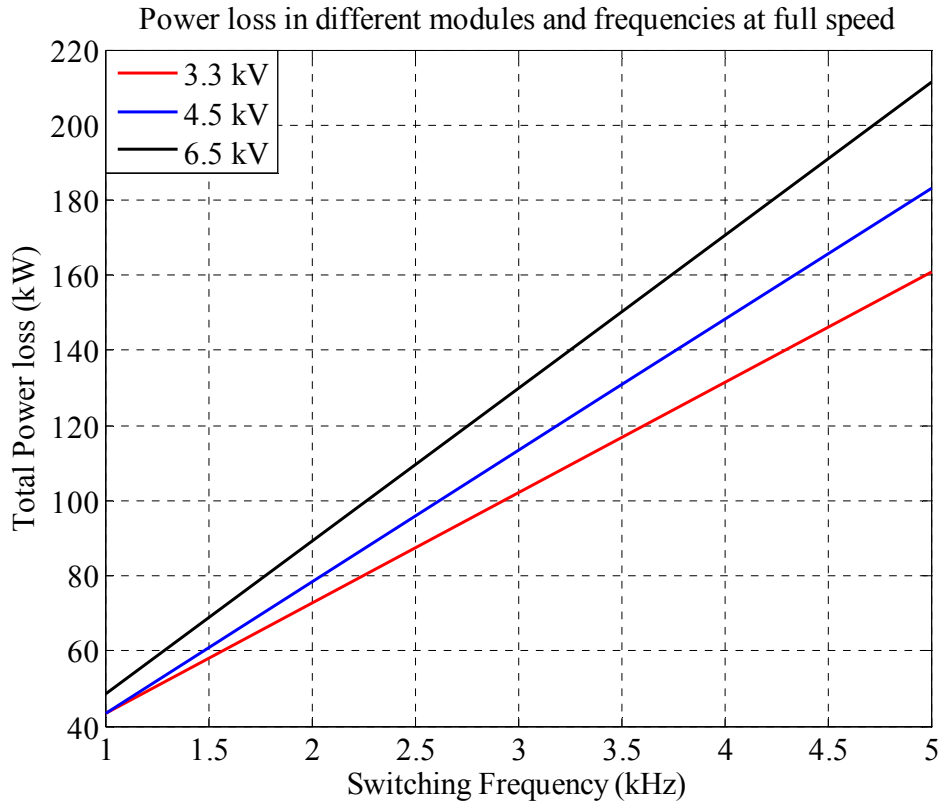


Figure 4.2: Power loss in different IGBT modules and frequencies at full speed (12-25 m/s).

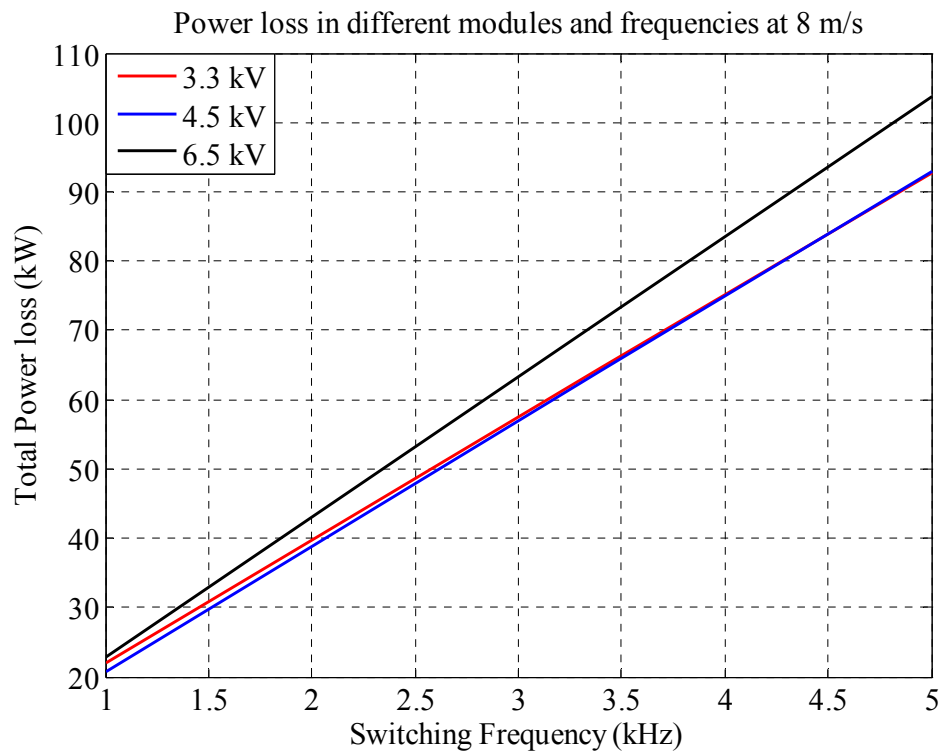
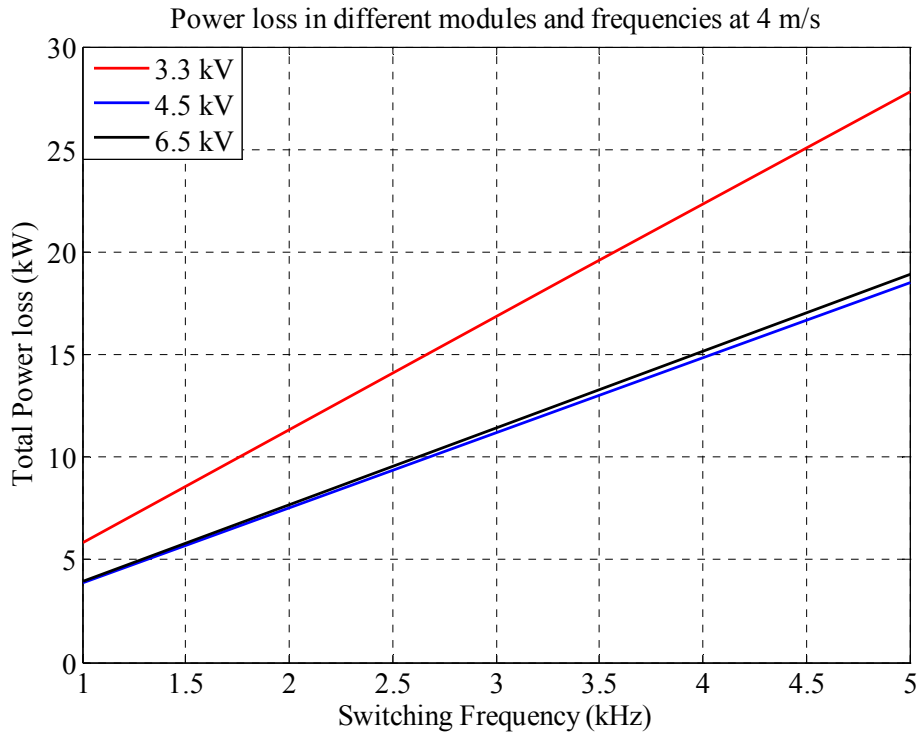
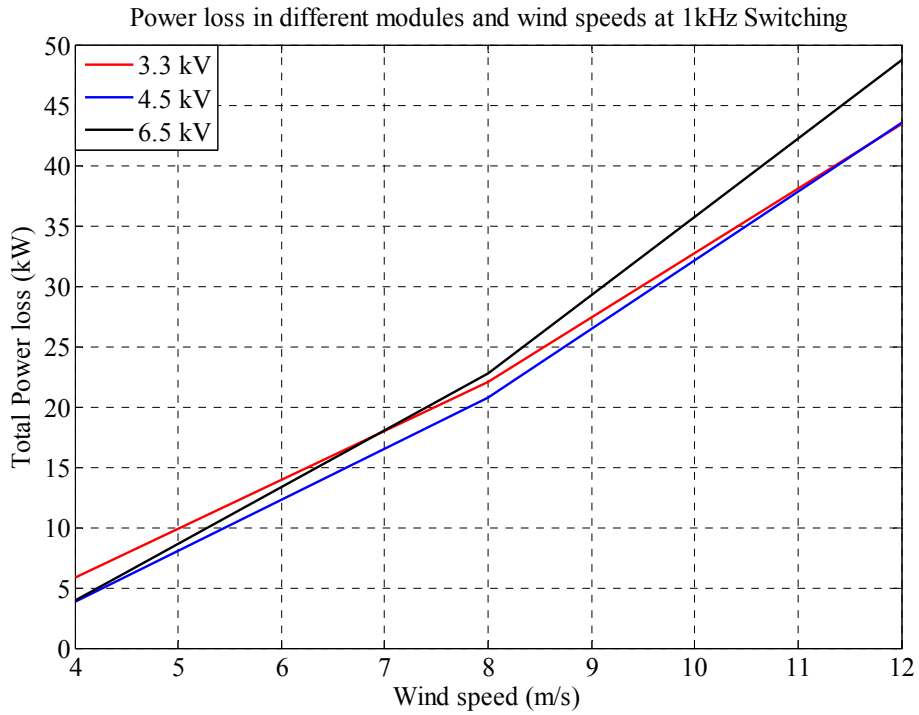


Figure 4.3: Power loss in different IGBT modules and frequencies at 8 m/s.



**Figure 4.4:** Power loss in different IGBT modules and frequencies at 4 m/s.



**Figure 4.5:** Power loss in different IGBT modules and wind speeds with 1 kHz switching frequency.

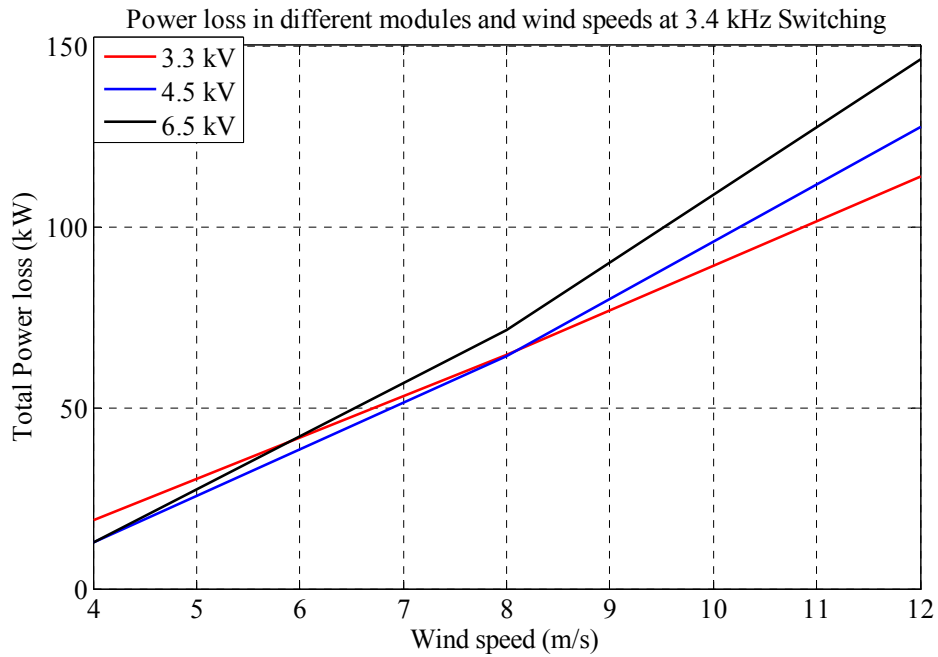


**Figure 4.6:** Power loss in different IGBT modules and wind speeds with 3.4 kHz switching frequency.

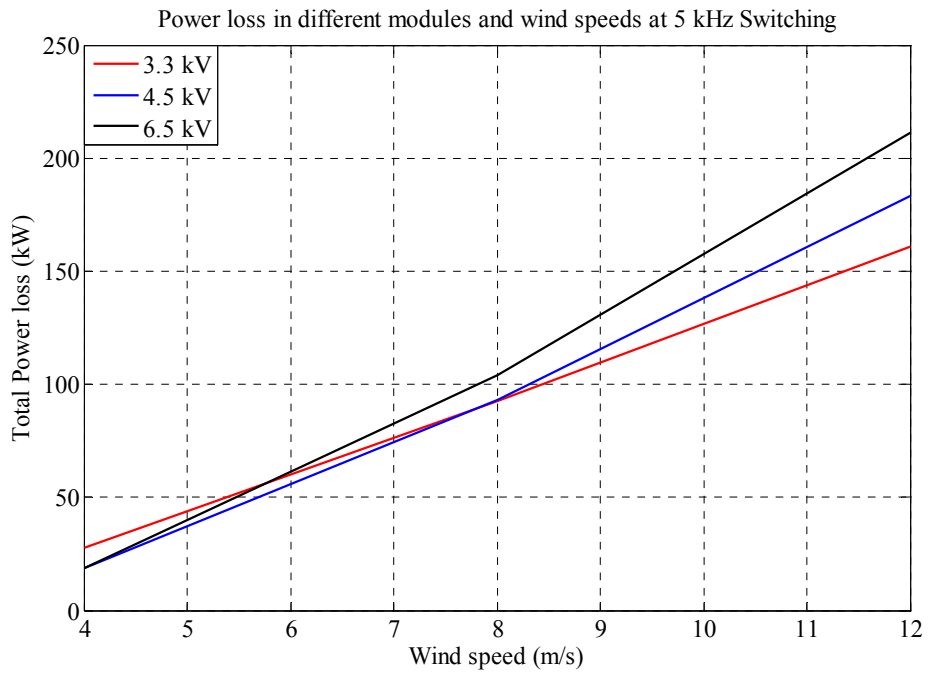


**Figure 4.7:** Power loss in different IGBT modules and wind speeds with 5 kHz switching frequency.

### Efficiency with switching frequency $f_{sw} = 1 \text{ kHz}$

$$P_{in} = 4.125 \text{ MW}$$

- For 3.3 kV module:

$$P_{loss} = 29341.94 + 14071.27 = 43413.21 \text{ W}$$
$$\eta = \left(1 - \frac{P_{loss}}{P_{in}}\right) \times 100\% = \mathbf{98.95\%}$$

- For 4.5 kV module:

$$P_{loss} = 34953.14 + 8562.05 = 43515.19 \text{ W}$$
$$\eta = \left(1 - \frac{P_{loss}}{P_{in}}\right) \times 100\% = \mathbf{98.94\%}$$

- For 6.5 kV module:

$$P_{loss} = 40656.66 + 8085.23 = 48741.89 \text{ W}$$
$$\eta = \left(1 - \frac{P_{loss}}{P_{in}}\right) \times 100\% = \mathbf{98.82\%}$$

### Efficiency with switching frequency $f_{sw} = 3.4 \text{ kHz}$

$$P_{in} = 4.125 \text{ MW}$$

- For 3.3 kV module:

$$P_{loss} = 99762.62 + 14063.26 = 113825.88 \text{ W}$$
$$\eta = \left(1 - \frac{P_{loss}}{P_{in}}\right) \times 100\% = \mathbf{97.24\%}$$

- For 4.5 kV module:

$$P_{loss} = 118840.68 + 8562.05 = 127402.73 \text{ W}$$
$$\eta = \left(1 - \frac{P_{loss}}{P_{in}}\right) \times 100\% = \mathbf{96.91\%}$$

- For 6.5 kV module:

$$P_{loss} = 138232.63 + 8085.23 = 146317.86 \text{ W}$$
$$\eta = \left(1 - \frac{P_{loss}}{P_{in}}\right) \times 100\% = \mathbf{96.45\%}$$

### Efficiency with switching frequency $f_{sw} = 5 \text{ kHz}$

$$P_{in} = 4.125 \text{ MW}$$

- For 3.3 kV module:

$$P_{loss} = 146710.00 + 14063.60 = 160773.60 \text{ W}$$
$$\eta = \left(1 - \frac{P_{loss}}{P_{in}}\right) \times 100\% = \mathbf{96.10\%}$$

- For 4.5 kV module:

$$P_{loss} = 174766.00 + 8562.00 = 183328.00 \text{ W}$$
$$\eta = \left(1 - \frac{P_{loss}}{P_{in}}\right) \times 100\% = \mathbf{95.55\%}$$

- For 6.5 kV module:

$$P_{loss} = 203279.00 + 8085.20 = 211364.20 \text{ W}$$
$$\eta = \left(1 - \frac{P_{loss}}{P_{in}}\right) \times 100\% = \mathbf{94.88\%}$$



## 5 Conclusions

In this thesis, three different IGBT ABB HiPak modules (3.3 kV, 4.5 kV and 6.5 kV) were used for the design of the active rectifier. Also, three different switching frequencies were tested with each module. After comparing the results, we conclude that the 6.5 kV module is the one with more losses, since it was the one with highest switching energy.

By switching with a lower frequency, the efficiency of the converter increases. Since at lower switching frequency, there are fewer losses.

The power factor of the converter can be increased if the design of the generator is improved, since it has a large air-gap reactance.

The switching losses are higher than the conduction losses in the active rectifier and this is because of the components that are being used for the converter. The switching losses are higher than conduction losses in the IGBT.

With the active rectifier, the generator torque can be fully controlled and the terminal voltage adjusted within certain limits.

The efficiency of the active rectifier is in the range between 95% and 99% which is a very good solution for an off-shore wind turbine with a PMSM working as a generator.



## **6 Future Work**

For this project, additional tasks can be done in order to evaluate better the performance of this type of converter. These include the thermal and cost analysis of the converter. Then, these results can be compared with previous rectifier topologies like diode or thyristor rectifiers.

Some other works that can be done in the future are the design of this same active rectifier in closed-loop control, to design an active rectifier with an electrically magnetized synchronous machine working as a generator, and design a DC-DC converter after the DC-link for both cases (EMSM and PMSM) for HVDC application.



## 7 Bibliography

- [1] **Anaya-Lara, Olimpo; Jenkins, Nick; Ekanayake, Janaka; Cartwright, Phill; Hughes, Mark.** *Wind Energy Generation, Modelling and Control*. UK : John Wiley & Sons, 2009. 978-0-470-71433-1.
- [2] **Hau, Erich.** *Wind Turbines. Fundamentals, Technologies, Application, Economics*. Berlin : Springer-Verlag, 2006.
- [3] **Manwell, J. F.; McGowan, J. G.; Rogers, A. L.;** *Wind Energy Explained. Theory, Design and Application*. UK : John Wiley & Sons, Ltd, 2009.
- [4] **Jha, A. R.;** *Wind Turbine Technology*. Boca Raton, FL : Taylor & Francis Group, LLC, 2011.
- [5] *Sustainable energy systems with HVDC transmission.* **Asplund, Gunnar;** Denver, CO : IEEE, 2004.
- [6] **Larruskain, D.M.; Zamora, I.; Mazón, A.J.; Abarrategui, O.; Monasterio, J.;** Solarec Egypt. [www.solarec-egypt.com/publications.html](http://www.solarec-egypt.com/publications.html). [Online] May 2005.
- [7] *Comparative Evaluation of HVDC and HVAC Transmission Systems.* **Meah, Kala; Ula, Sadrul;** Laramie, WY : IEEE, 2007.
- [8] **Stiebler, Manfred;** *Wind Energy Systems for Electric Power Generation*. Berlin : Springer-Verlag, 2008.
- [9] **Ackermann, Thomas.** *Wind Power in Power Systems*. UK : John Wiley & Sons, Ltd, 2005.
- [10] **Lundberg, Stefan.** *Configuration Study of Large Wind Parks*. Göteborg : Chalmers University of Technology, 2003.
- [11] *A Review Of Three-Phase Improved Power Quality AC-DC Converters.* **Singh, Bhim; Singh, Brij N.; Chandra, Ambrish; Al-Haddad, Kamal; Pandey, Ashish; Khotari, Dwarka P.** 3, Delhi, India : IEEE, 2004, Vol. 51. 0278-0046/04.
- [12] **García Colino, Sergio.** *DC High Voltage Connection Systems for Offshore Wind Turbines*. Göteborg : Chalmers University of Technology, 2010.
- [13] **Marques, André Madeira.** *Design, Control, Simulation and Energy Evaluation of a DC Offshore Wind Park*. Lisbon : Instituto Superior Técnico, Universidade Técnica de Lisboa, 2009.
- [14] **Rashid, Muhammad H.** *Power Electronics Handbook, Devices, Circuits and Applications*. Oxford : Elsevier Inc., 2007.
- [15] *Status of the techniques of three-phase rectifier systems with low effects on the mains.* **Kolar, J.W.; Ertl, H.;** New York : IEEE INTELEC, 1999.
- [16] **Kazmierkowsky, Marian P., Blaabjerg, Frede y Krishnan, Ramu.** *Control in power electronics. Selected Problems*. San Diego, CA : Elsevier Science, 2002.

- [17] **IXYS;** IXYS. *Power Semiconductors Application Notes*. [Online] IXYS Corporation, 2007. [Cited: July 24, 2011.]  
[http://www.ixyspower.com/tech\\_support/application\\_notes.html#IGBTs](http://www.ixyspower.com/tech_support/application_notes.html#IGBTs).
- [18] **Mogstad, Anne Berit.** *New Switching Pattern for AC/AC Converters With RB-IGBTs for Offshore Wind Parks*. Trondheim : Norwegian University of Science and Technology, 2008.
- [19] **Mohan N., Undeland T., Robbins W.** *Power Electronics, Converters, Applications and Design*. USA : John Wiley & Sons, Inc., 1995.
- [20] *Future of electrical machines and drives*. **Vas, P.; Drury, W.;** Vigo, Spain : ICEM, 1996.
- [21] **Nasar, S.A.;** *Handbook of Electric Machines*. New York : McGraw Hill, 1987.
- [22] **Ahmad, Mukhtar.** *High performance AC Drives. Modelling Analysis and Control*. London : Springer, 2010.
- [23] *Control of Permanent Magnet Synchronous Generator for Large Wind Turbines*. **Busca, Cristian; Stan, Ana-Irina; Stanciu, Tiberiu; Stroe, Daniel Ioan;** Aalborg, Denmark : Department of Energy Technology, Aalborg University, 2010.
- [24] **Marinowsky, Mariusz;** *Sensorless Control Strategies for Three-phase PWM Rectifiers*. Warsaw, Poland : Warsaw University of Technology, 2001.
- [25] **Cimpoeru, Andreea.** *Encoderless Vector Control of PMSG for Wind Turbine Applications*. Pontoppidanstraede : Institute of Energy Technology, Aalborg Universitet, 2010.
- [26] **Lundberg, Stefan;** *Lecture slides from Electric Drives II course*. [Lecture slides] Göteborg : Chalmers University of Technology, 2011.
- [27] **Gieras, Jacek F.; Wing, Mitchell;** *Permanent Magnet Motor Technology. Design and Application*. New York : Marcel Dekker, Inc., 2002.
- [28] **Chalmers University of Technology.** Other Publications. [Online] Cited: August, 2011.  
<http://www.chalmers.se/ee/SV/forskning/forskargrupper/elteknik/publikationer/ovriga-publikationer>.
- [29] **Electric-Driver.** Power Semiconductor Application. Semisel. [Online] Cited: September, 2011. <http://www.electric-driver.com/%E4%BA%A7%E5%93%81/%E6%8A%80%E6%9C%AF%E4%BA%A7%E5%93%81/%E7%94%B5%E5%8A%9B%E7%94%B5%E5%AD%90%E5%9F%B A%E7%A1%80%E7%9F%A5%E8%AF%86.pdf>